Narrow-linewidth External Cavity Diode Lasers for Atomic Physics

T.B.M. van Leent

January 15, 2017

Abstract

We developed a series of tunable, narrow-linewidth, external cavity diode lasers (ECDLs) for applications in atomic physics. These applications include spectroscopy, laser cooling and trapping of strontium, as well as the creation of atom-optics elements. Our approach is to isolate the ECDL from external disturbances, such as temperature changes, sound, or vibrations. We use a massive laser housing with high heat capacity, which we decouple from the environment thermally and acoustically. We demonstrate a *blue* ECDL with a wavelength of 461 nm that has a free-running frequency drift of < 30 MHz/h. The laser is locked to the $^1S_0 \rightarrow {}^1P_1$ transition in strontium and stays locked for >1 day. Also, we demonstrate a *red* ECDL with a wavelength of 689 nm with a free-running linewidth of 443 kHz (Voight FWHM). The noise of the laser is further characterized by measuring the power spectral density.

Acknowledgements

First of all I want to thank Florian Schreck for giving me the opportunity to work in his strontium quantum gas group. It was a very inspiring group to work in with highly motivated people, people that really have passion for what they are doing. It was a great experience to be part of this.

I would like to thank Shayne Bennetts, my daily supervisor, although, daily may not be the right word here. Do not understand me wrong, because we did speak with each other on a daily basis, but nightly would have been a better fit. Nevertheless, I would not have wanted another daily supervisor. Shayne believes that during a master project a student should learn how to work with all different aspects of doing research in an optics lab (optics, vacuum, design software, electronics, etc.). He planned a versatile year for me in which I could learn a lot and experience how it is to be a researcher. Also, there are not many people who are so passionate about their job as Shayne. If you do not believe me try asking him what kind of machine he wants to built next. His passion for physics motivated me the whole year.

If I have to name someone in the group that is most willing to help its Chun-Chia Chen. Before I could finish my question Chun-Chia was already running to the condensed matter hall to find the tool I was looking for. For every problem about the electronics I could rely on his knowledge.

Next I want to thank Benjamin Pasquiou, the last not yet mentioned SrCAL team member. Benjamin greatly helped me with the spectroscopy lock.

I would also like to thank the staff of the Technical Workshop, especially Jan Kalwij, for their excellent work in manufacturing all the designs.

Further, I would like to thank Alessios Ciamei for the help with the heterodyne beat note setup, Oleksiy Onischenko for his feedback on the manuscript, and Alex Bayerle for sharing his knowledge about ECDL electronics.

Contents

Abstract **i**

Acknowledgements **ii**

Contents **v**

1 Introduction **1**
1.1 Lasers 1
1.2 Applications of Narrow-linewidth Lasers in Strontium Quantum Gases 3
1.3 Constructing Narrow-linewidth Tunable Lasers 5
1.4 Our Approach 6
1.5 Thesis Overview 6

2 Diode Lasers **8**
2.1 Basic Concepts 8
2.2 Creating the External Cavity 9
2.2.1 Grating in Littrow Configuration 11
2.2.2 Parameters Grating and Collimator 12
2.2.3 Cavity Length 13
2.3 Mode Selection 13
2.4 Mode-hop Free Tuning 15

3 ECDL Design and Construction **18**
3.1 Design 18
3.1.1 Housing 18
3.1.2 Optical Configuration 20
3.1.3 Opto-mechanical Configuration 22
3.1.4 Temperature Control 26
3.1.5 Electronic Drivers 29
3.1.6 Alternative Flexure Design 32

3.2 Construction . . . 33
3.2.1 Optical Alignment . . . 33
3.2.2 Optimization of the Wavelength . . . 34

4 Absolute Frequency Stabilization 36
4.1 Doppler-free Saturated Absorption Spectroscopy . . . 36
4.2 Modulation Transfer Spectroscopy . . . 38
4.3 Assembling the Spectroscopy Cell . . . 39
4.4 Experimental Setup . . . 41
4.5 Results . . . 46
4.5.1 Recommendations to Increase Error Signal . . . 46
4.6 Locking Procedure . . . 48

5 Linewidth and Phase Noise Spectrum 49
5.1 Noise in the Time and Frequency Domain . . . 50
5.2 Types of Noise . . . 51
5.3 Linewidth Measurement Technique . . . 52
5.3.1 Heterodyne Beat Note . . . 52
5.3.2 Reference Laser . . . 54
5.3.3 Balanced Detection . . . 54
5.3.4 Alternative Linewidth Measurement Techniques . . . 54
5.4 Experimental Setup . . . 54
5.4.1 Beat Lock . . . 55
5.5 High Frequency Linewidth Measurement . . . 56
5.6 Low Frequency Linewidth Measurement . . . 58
5.6.1 Time Averaging the PSD . . . 58
5.6.2 Scaling the PSD . . . 59
5.6.3 PSD Measurements . . . 59
5.6.4 PSD to Linewidth . . . 60
5.7 Discussion . . . 61
5.7.1 Sidebands Reference Laser . . . 61
5.7.2 Grating Mount Resonance Frequencies . . . 61

6 Summary and Outlook 64
6.1 Summary . . . 64
6.2 Outlook . . . 65

A Circuit Diagrams 66
A.1 Current Controller . . . 66
A.2 Temperature Controller . . . 66
A.3 PID . . . 66

A.4 Connector 66

B Matlab Code PSD **67**
B.1 Read 67
B.2 Process data 68
B.3 Scale and Plot 69

C Drawings of Designs **72**
C.1 ECDL Housing 72
C.2 Flexure Grating Mount 72
C.3 CMM Grating Mount 72

Chapter 1

Introduction

1.1 Lasers

The first laser was built in 1960 by Maiman [1], and, ever since, extensive theoretical and experimental research has been conducted in the field of laser physics. Nowadays the laser has many (critical) applications, and it is hard to imagine a world without. Applications include imaging, eye surgery, chip fabrication, and industrial cutting and welding. Or try to imagine the queue in a supermarket without bar-code scanning.

A laser is a device that produces spatially and temporally coherent light. The coherence originates from optical amplification by stimulated emission, theoretically described by Einstein in 1917 [2] and illustrated in Figure 1.1.1. In this process a photon traveling through a medium stimulates the emission of a second photon with identical direction and frequency.

Lasing is achieved when sufficient gain is provided by stimulated emission to overcome losses. By pumping energy into the gain medium, population inversion between two energy levels can be created. Pumping above a threshold

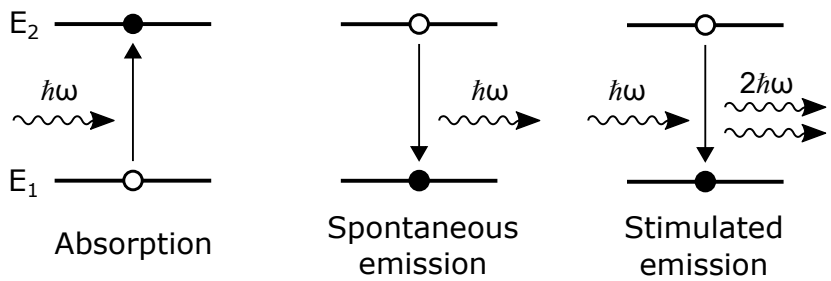

Figure 1.1.1: **Optical transitions in a two-level atom.** Optical amplification in a laser arises from stimulated emission.

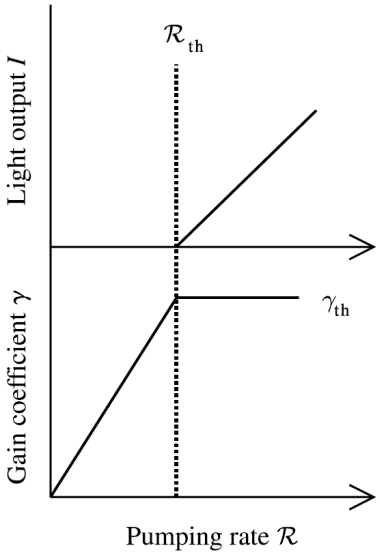

Figure 1.1.2: **Laser threshold.** Pumping treshold for lasers. *Figure copied from reference [3]*

value results in a net optical gain, as illustrated in Figure 1.1.2.

The emission spectrum of a laser is defined by the energy difference between the high (E_2) and low (E_1) energy state of the gain medium and has a modal structure [4]. The modal structure is introduced by placing the gain medium in an optical cavity. Photons are captured in cavity modes and therefore circulate through the gain medium multiple times while being optically amplified. The different lasing modes compete against each other, giving rise to instability and mode-hops. By selectively favoring one of the modes, single mode lasing can be achieved and tunability arises by manipulating this mode. Figure 1.1.3a shows a schematic of a laser where energy is pumped into the gain medium (G), and therefore photons are emitted by spontaneous emission in random directions. Photons emitted into cavity modes of the mirrors (M) will circle through the gain medium multiple times while being optically amplified by stimulated emission. Figure 1.1.3b illustrates the emission spectrum of the gain medium and the cavity modes introduced by the optical cavity.

Linewidth is one of the key parameters that characterizes a laser; it quantifies the spectral purity of the emitted light. The linewidth of a laser is bounded from below by fundamental quantum noise, as theoretically described by Schawlow-Townes in 1958 [6]. However, the linewidth of most lasers greatly exceeds this limit because of classical noise originating from mechanical vibrations in the optical resonator, pump power fluctuations, or

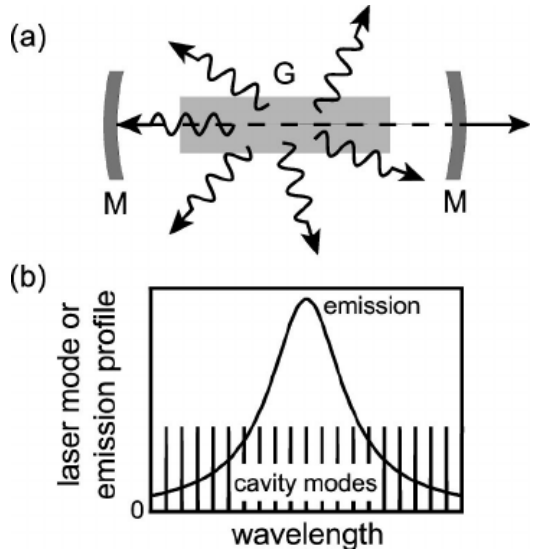

Figure 1.1.3: **Schematic of a laser and the cavity modes introduced by the optical cavity. a)** Simple schematic of a laser with gian medium (G) within an optical cavity formed by the mirrors (M). **b)** Emmision spectrum of the gain medium and the cavity modes introduced by the optical cavity. *Figure copied from reference [5]*

temperature fluctuations. Nowadays there are many applications that require tunable narrow-linewidth lasers, including frequency metrology [7], optical clocks, optical communication [8, 9], high resolution spectroscopy, and laser cooling and trapping [10].

1.2 Applications of Narrow-linewidth Lasers in Strontium Quantum Gases

The goal of this project is to develop a series of stable, tunable, and narrow-linewidth lasers. We will implement the lasers within the strontium continuous atom laser (SrCAL) project. Applications within the project include laser cooling and trapping, and non-destructive imaging, which we will briefly introduce in the following paragraphs.

Strontium can be laser cooled to quantum degeneracy by driving two transitions [11]. The *blue* 461 nm $^1S_0 \rightarrow {}^1P_1$ transitions with a broad-linewidth of 30.5 MHz and the *red* 689 nm $^1S_0 \rightarrow {}^3P_1$ transition with a narrow-linewidth of 7.4 kHz, as illustrated in Figure 1.2.1. Nowadays cooling to quantum degeneracy is a process consisting of two incompatible steps: laser cooling

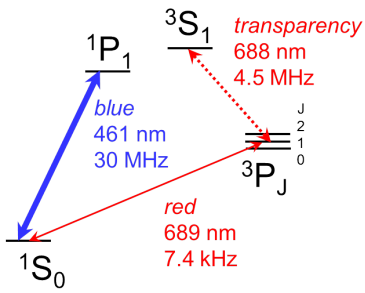

Figure 1.2.1: **Simplified energy level scheme strontium.**

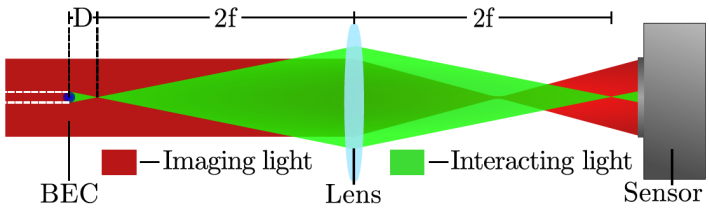

Figure 1.2.2: **Schematic non-destructive phase contrast imaging.** *Figure copied from reference [13]*

followed by evaporative cooling while protected from scattered photon heating. However, when the two laser cooling stages of strontium are separated in space, in combination with a *transparency* beam, it is theoretically possible to create a continuous atom laser with a high flux of coherent atoms (i.e. a continuous source of matter-waves). The lasers developed during this project will be used to drive both cooling transitions in strontium.

Ultracold matter-waves can be probed with optical diagnostics. Absorption, fluorescence and dispersive light-matter interactions form the basis for the optical diagnostics techniques. For non-destructive imaging the amount of heat added to the condensate should be minimized. Dispersive imaging gives two orders of magnitude more signal for the same amount of heat produced compared to absorption or fluorescence imaging [12]. Therefore, it is possible to take real-time movies of 100 frames instead of capturing a single frame. Partial phase contrast imaging is such a method, a schematic of non-destructive phase contrast imaging is given in Figure 1.2.2. A narrow-linewidth laser is needed to precisely detune light from the atomic resonance.

Gain medium	Typical Properties	Advantages and Limitations
Dye	400-1000 nm Efficiency 10-30%	Changeable gain medium; Tunable over 1-300 nm; Simple construction; Expensive
Solid state	Efficiency 1-10%	High peak power; High pulse energy
Semiconductor	400-2000 nm Efficiency 50%	Compact; Cheap; Tunable over typically 15 nm
Fiber	Efficiency 25-35%	Narrow-linewidth; High average power; Not suitable for Q-switching; Limited range of frequencies

Table 1.1: **Some characteristics of different laser technologies.**

1.3 Constructing Narrow-linewidth Tunable Lasers

Traditionally, tunable dye lasers were the workhorse in many physics labs. However, since the first external cavity diode laser (ECDL) designs were developed in the early 1980s, the popularity of the diode laser increased steadily [14] [15]. This process was driven by the steadily increasing range of available powers and wavelengths from single spatial mode diodes, a process which continues today. A comparison of advantages and limitations for dye, solid-state, semiconductor and fiber lasers is given in Table 1.1.

In ECDLs tunability and narrow-linewidth originate from frequency selective optical elements in the external cavity. The theory is well understood and extensive literature on various designs exists. Interference filter-stabilized ECDLs designs have been reported that achieve linewidths of less than 85 kHz [16]. However, most commonly, a diffraction grating in a Littrow or a Littman-Metcalf configuration is used to provide selective optical feedback to the diode. Easily machined and compact designs are described that offer single-mode operation with a linewidth of a few 100 kHz and 25 GHz of mode-hop free tuning [17]. In Littrow configuration linewidths below 100 kHz have been demonstrated [18]. Recently, tuning ranges of 200 nm and 5 kHz linewidth have been reported [19]. Also, ECDLs with a footprint as small as 10x5 mm have been reported in literature [20].

Commercial designs are a compromise between tunability and stability.

However, we can optimize our design for our requirements; for example, by sacrificing tunability or compactness for stability. One design challenge is maintaining stable single mode output in the presence of external environmental perturbations; how can we optimize the design to improve stability. Our goal is to develop a laser that can be locked to narrow transitions with improved long term stability and lower cost compared to commercial systems.

1.4 Our Approach

In the lab, laser delocking due to instability is the most common problem. If lasers delock during an hour-long search for fine features, the whole dataset usually needs to be retaken. This wastes countless hours of machine time slowing progress and dramatically reducing lab efficiency.

Our approach is to reduce these instabilities by minimizing thermal fluctuations and mechanical vibrations in the laser. Thermal fluctuations are reduced by using a massive laser housing with high heat capacity, passive thermal insulation, and active thermal control. Mechanical vibrations are suppressed by a stiff design and acoustic isolation.

Mounting the grating on a standalone part makes it possible to operate with different ECDL configurations optimized for various requirements (stability, tunability, linewidth, wavelength etc.) and to change the external cavity length. In ECDLs the theoretical linewidth depends on the free parameters of the design, such as grating spacing and external cavity length. By reducing classical noise in the driving current, mechanical vibrations, and thermal instabilities we aim to reduce the actual linewidth to a value approaching this theoretical limit.

Developing our own laser system will better fit the needs of our experiments, and, in case of failure, we are not dependent on a third party. Also, since strontium has many interesting transitions, we can cost-effectively develop multiple lasers that address these different transitions.

1.5 Thesis Overview

This thesis is organized as follows. In Chapter 2 we will present the basic theory of an external cavity diode laser. Chapter 3 then introduces a general ECDL design, including grating mount designs focused on tunability (the *blue* ECDL) or narrow-linewidth (the *red* ECDL). Also, basic characteristics of the lasers are discussed. In Chapter 4 we discuss the absolute frequency stabilization of the *blue* ECDL to an atomic transition in a gas of strontium.

In Chapter 5 we discuss linewidth measurements and phase noise spectra of the *red* ECDL. Finally, in Chapter 6, we will give a summary and outlook including recommendations to improve the current design.

Chapter 2

Diode Lasers

The physics of semiconductor lasers has been extensively studied and many references exist [4, 21, 22]. In the previous chapter we discussed fundamental properties of lasers in general, such as optical amplification, lasing modes, threshold, emissions spectrum and linewidth. In addition, in Section 2.1 we will discuss key properties of semiconductor lasers in specific. In Section 2.2 we will introduce the external cavity with dispersive optical feedback, which makes it possible to achieve narrow-linewidth and single mode lasing. Also, we will discuss the free parameters in the design for an external cavity diode laser (ECDL). In Section 2.3 we will present a theoretical model of the mode selection in an ECDL. Finally, in Section 2.4 we will discuss the mode-hop free tuning range and give an approach to maximize this range.

2.1 Basic Concepts

In diode lasers the optical amplification originates from electronically pumping a p-n junction in a semiconductor material. The pumping produces electrons and holes which recombine and emit photons. The band gap between the valence and conduction band sets the center frequency of the emitted light, the light has a typical linewidth of a few nm. By adding a dielectric coating to the diode facets they will act as mirrors and an optical cavity is formed.

Laser diodes typically have an elliptical and diverging beam profile. This originates from the size of the diode and the layered structure needed to produce the p-n junction, as illustrated in Figure 2.1.1. The spatial lasing mode is confined by gain or refractive index variation in the active layer [14]. Nevertheless the mode is asymmetric in the directions parallel and perpendicular to the active layer.

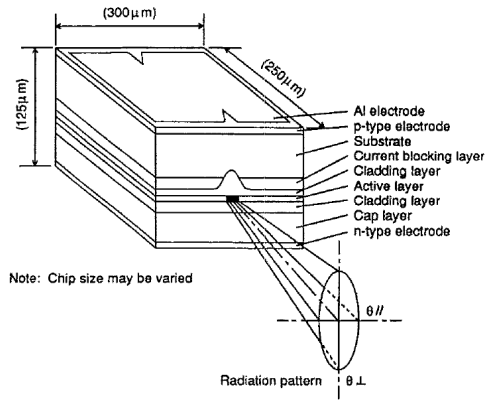

Figure 2.1.1: **Schematic different layers and beam profile diode.** *Figure is copied from reference [14].*

The threshold current of diode lasers depends on temperature [4]. To achieve lasing enough electrons must be pumped to the conduction band to provide sufficient gain to overcome losses. The pumping efficiency depends on temperature and therefore the threshold current depends on temperature. This is illustrated for a typical diode laser in Figure 2.1.2.

An empirical approach shows that the band gap energy of a semiconductor is dependent on temperature via the Varshni equation [23]. Intuitively this can be understood in the following way; an increase in temperature results in an expansion of the semiconductor material, this effectively reduces the potential energy of the electrons in the semiconductor, and therefore reduces the band gap energy. In Figures 2.1.3 and 2.1.4 this relationship is illustrated since the band gap is directly related to the emission wavelength of the diode.

2.2 Creating the External Cavity

Narrow-linewidth and single-mode lasing of a diode can be achieved by adding an external cavity including a dispersive optical element. By selective optical feedback the diode can be tuned through its broad gain curve. Most commonly, the dispersive feedback is introduced by adding a diffraction grating in the Littrow configuration [17, 24]. The Littrow configuration is often favored because it is very simple, i.e. only a grating is added.

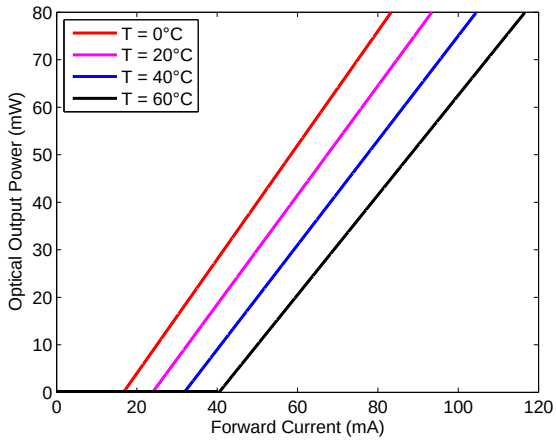

Figure 2.1.2: **Optical output power vs forward current.** Typical laser diode forward currents and optical output powers for different temperatures.

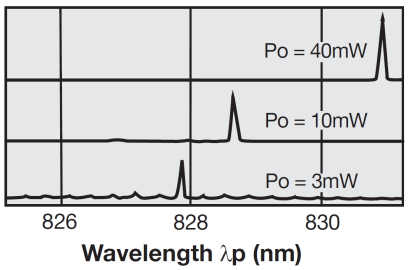

Figure 2.1.3: **Optical output power for a varying forward current.** Quantities for a typical laser diode. *Figure copied from Schafter+Kirchoff Physics Fundamentals: Laser Diode Characteristics.*

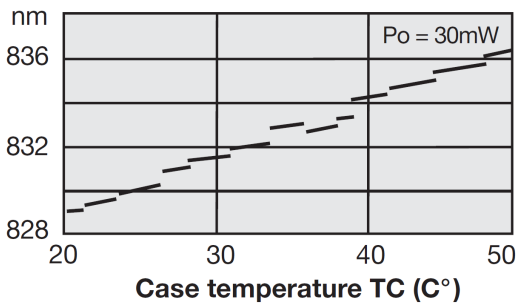

Figure 2.1.4: **Emissions wavelength for a varying temperature.** Quantities for a typical laser diode. The discontinuities represent mode-hops of the laser. *Figure copied from Schafter+Kirchoff Physics Fundamentals: Laser Diode Characteristics.*

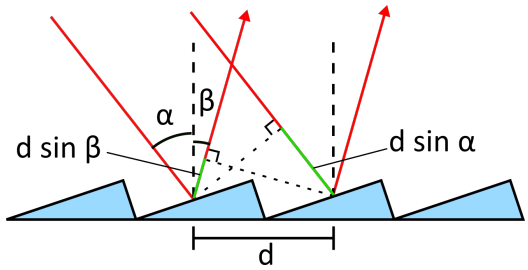

Figure 2.2.1: **Diffraction from a grating.** The angle of the incident and diffracted beam are labeled α and β respectively. The grating pitch equals d. The path length differences between the two beams diffracted from adjacent grating grooves are indicated in green.

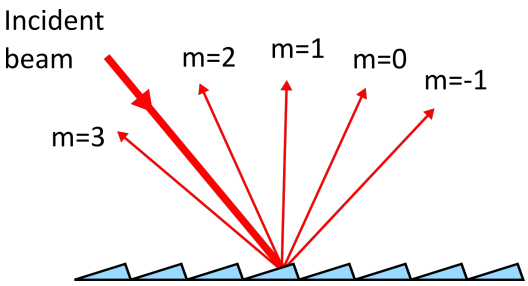

Figure 2.2.2: **Diffraction orders for a collimated and monochromatic beam.**

2.2.1 Grating in Littrow Configuration

Let us first derive the grating equation. Lets assume a collimated monochromatic beam of wavelength λ that reflects from a grating with grating pitch d. We will name the angle of the incident and diffracted beam α and β respectively, as indicated in Figure 2.2.1. Now a path length difference arises between light that is reflected from adjacent grating grooves. For the incident beam the path length difference equals $d \sin \alpha$, while the diffracted beam path length difference equals $d \sin \beta$. For constructive interference of the diffracted beams the total path length difference must be an integer multiple of the wavelength. Hence, we obtain the grating equation

$$m\lambda = d \sin \alpha \pm d \sin \beta, \tag{2.2.1}$$

where m is an integer. Since the angle of diffraction is wavelength dependent, we can selectively reflect a specific wavelength back to the diode. In Figure 2.2.2 the different orders of diffraction are illustrated for a collimated monochromatic beam.

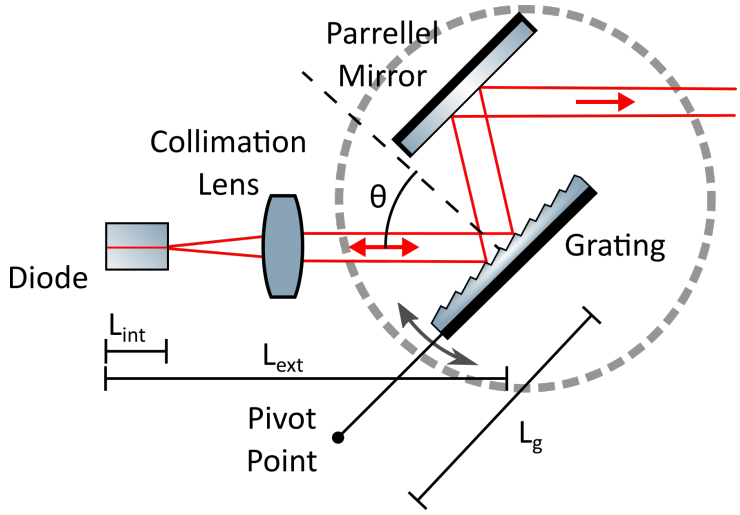

Figure 2.2.3: **Geometry ECDL in Littrow configuration.** The internal and external laser cavity lengths are labeled by L_{int} and L_{ext} respectively. The grating arm length equals L_g. The grating angle is labeled by θ and is equal to the Littrow angle.

Now the Littrow configuration is as follows. The first order reflection ($m = 1$) of the diffraction grating is reflected back to the diode and is used as optical feedback, the zero order reflection ($m = 0$) becomes the output beam of the laser. We can rewrite Equation 2.2.1 for $m = 1$ and $\alpha = \beta = \theta_{Littrow}$ and hence obtain the Littrow angle

$$\theta_{Littrow} = \sin^{-1}(\frac{\lambda}{2d}). \tag{2.2.2}$$

Frequency tuning is achieved by rotating the grating and therefore changing the optical feedback to the diode. Because this rotation also changes the output beam direction an additional mirror is placed parallel to the grating, as proposed by Hawthorn *et al.* [25]. The Littrow configuration with added parallel mirror for fixed output direction is illustrated in Figure 2.2.3.

2.2.2 Parameters Grating and Collimator

The parameters of the grating and collimator, such as, grating pitch, numerical aperture, and focal length, have some decision freedom. We will derive an equation for dispersion from a grating to gain insight how these parameters influence the output beam. Therefore, we fix the angle of incidence in the grating equation (Equation 2.2.1) and take its derivative with respect to wavelength. Hence we obtain

$$m\,d\lambda = d\cos\beta\,d\beta. \tag{2.2.3}$$

The angular dispersion D is defined as a change of diffraction angle over a small change of wavelength. Combining this with the equation above gives

$$D = \frac{d\beta}{d\lambda} = \frac{m}{d\cos\beta}. \tag{2.2.4}$$

Higher dispersion results in more precise optical feedback to the diode. Therefore, for narrow-linewidth lasing, a smaller grating pitch and larger Littrow angle are preferred.

Similarly, the grating resolution can be increased by increasing the beam size. However, increasing the grating resolution makes the optical feedback more sensitive to the grating angle perturbations. Therefore slight thermal drifts or mechanical instabilities make it difficult to maintain stable operation. Loh and coworkers pushed this limit and for them it was reached with a collimator of $f = 8$ mm and a grating $d = 1/1800$ mm^{-1} [26].

2.2.3 Cavity Length

When a passive region is added to the lasing cavity, i.e. an external cavity, the coherence time of the light in the lasing cavity increases. However, since the region is passive, no extra emission noise is added. In theory this can narrow the linewidth of an ECDL by the squared of the fraction of the cavity optical length of the active region [27]. Mathematically, this fraction is equal to

$$\eta = \left(\frac{t_{int}}{t_{int} + t_{ext}}\right)^2, \tag{2.2.5}$$

where t_{int} and t_{ext} are the round-trip time of the internal and external cavity respectively. For $L_{int} = 0.250$ mm and $L_{ext} = 40$ mm the linewidth will narrow by a factor of 1.2×10^4 assuming the same reflections. However, mechanical instabilities limit the cavity length, for longer cavities stable lasing can not be achieved [26].

2.3 Mode Selection

A useful way to describe circulating light in optical cavities is by resonator modes. By adding the grating, external cavity modes arise and we get more mode competition since the mode spacing is smaller compared to the internal cavity modes. Now, the modal behavior is dependent on the diode gain,

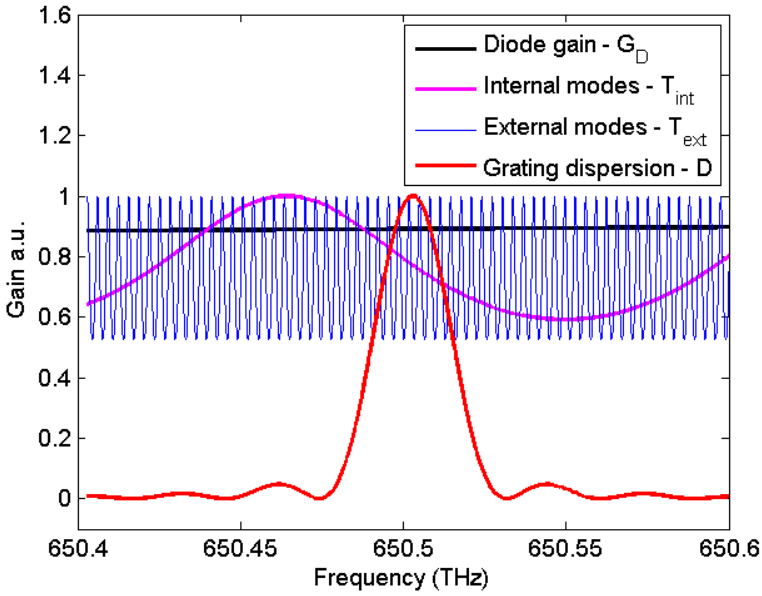

Figure 2.3.1: **Mode selection external cavity diode laser.** Mode selection following the approach by Saliba *et al.* [28]. Modeled around $\upsilon_0 = 461$ nm for $\sigma_{diode} = 5$ nm, $\upsilon_{diode} = 458$ nm, $d = 1/3600$ mm, $a = 1$ mm, $r_{rear} = 0.85$, $r_{front} = 0.02$, $r_{grating} = 0.03$, $n_{air} = 1$, $n_{diode} = 3.5$, $L_{int} = 0.250$ mm, and $L_{ext} = 47$ mm.

internal cavity, external cavity, and grating dispersion. Furthermore, these modes depend in different ways on cavity length, optical-feedback, and temperature. As a result, instabilities arise and mode-hops occur when the mode with maximum gain changes from one mode to another. A great challenge in the ECDL design is to overcome these instabilities and create large stable regions where the frequency can be tuned continuously.

Following the approach by Saliba *et al.* [28], we will look at the product of the frequency dependent gain and loss factors of an ECDL

$$T_{total} = G_D T_{int} T_{ext} D, \tag{2.3.1}$$

where G_D is the diode gain profile, T_{int} and T_{ext} are the transmission functions of the internal and external cavities respectively, and D represents the grating dispersion. Let us first find expression for these four factors.

The diode gain profile is approximated by a Gaussian with standard deviation σ_{diode} and center frequency υ_{diode} as

$$G_D = \exp\left[-\frac{(\upsilon - \upsilon_{diode})^2}{2\sigma_{diode}^2}\right]. \tag{2.3.2}$$

Since the medium gain profile is broad compared to the other factors in Equation 2.3.1 the precise shape is not crucial for the model.

The modes (or transmission functions) formed by the cavities are described by the Airy function [29]

$$T_x = \frac{1}{1 + F_x \sin^2(\delta_x(\upsilon)/2)}, \tag{2.3.3}$$

where

$$F_x = \frac{4\sqrt{r_{x1}r_{x2}}}{(1-\sqrt{r_{x1}r_{x2}})^2}, \qquad \text{and} \qquad \delta_x(\upsilon) = 4\pi n_x L_x \upsilon/c, \tag{2.3.4}$$

where $r_{x1,2}$ are the reflectivity's of the mirrors that form the cavity, n_x is the refractive index of the medium the light is traveling through, L_x is the cavity length, and c is the speed of light.

The selective optical-feedback by the grating can be evaluated from the diffracted intensity D. Assuming a square-slit profile this gives [29]

$$D = \left[\frac{\sin(kNd\sin\theta)}{N\sin(kNd\sin\theta)}\right]^2 \operatorname{sinc}^2\left(\frac{kd\sin\theta}{2}\right), \tag{2.3.5}$$

where k is the wavenumber, d is the grating spacing, $N = 2a/d$ is the number of grooves illuminated by the light, where $2a$ is the $1/e^2$ beam diameter, and, since we use the Littrow configuration for the grating, θ equals the Littrow angle.

The found expressions for the frequency dependent gain and loss factors of Equation 2.3.1 are plotted in Figure 2.3.1 for specific parameters. The mode where the product is maximum will be favored compared to other modes. In Figure 2.3.2 the product of the factors is plotted. Note that we will ignore the cavity formed between the front facet of the diode and the grating. Since both mirrors of this cavity have a low reflectivity the finesse will be low as well. As a result the gain curve will only slightly vary with frequency and can therefore be omitted.

2.4 Mode-hop Free Tuning

Following the theory presented in the previous subsection, the grating position affects the total transmission function in two ways. First, by its angle

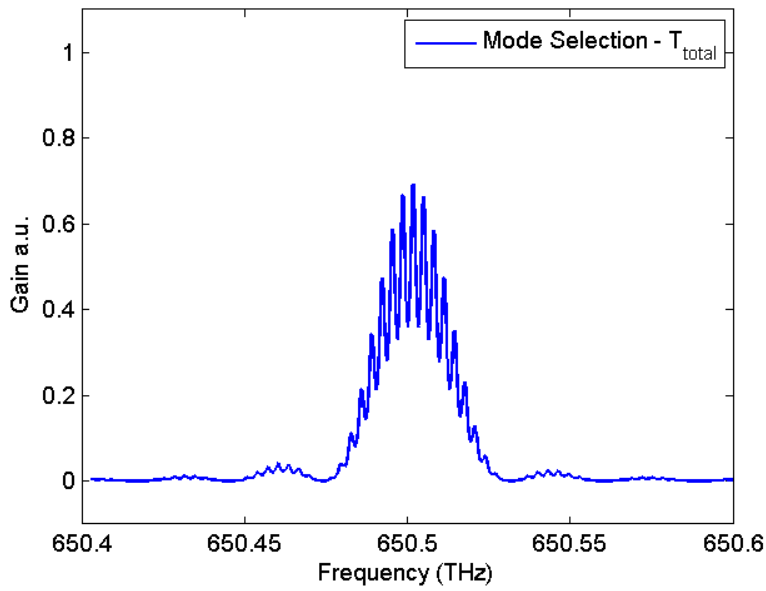

Figure 2.3.2: **Product frequency depedent gain and loss factors ECDL.** Plot of Equation 2.3.1 over frequency for the same parameters as used in Figure 2.3.1.

relative to the diode (υ_g). Second, by its distance relative to the diode (υ_{ext}). Frequency tuning can therefore be achieved in two ways as well; changing υ_g or υ_{ext}. However, to eliminate mode-hops, synchronous frequency tuning of both processes is required. To make the problem more concrete we introduce the geometry as proposed by Saliba *et al.* [28], as sketched in Figure 2.2.3. The frequency tuning by grating rotation is given by the following equations:

$$\upsilon_{ext} = \frac{mc}{2(L_{ext} - L_e)}, \tag{2.4.1}$$

and

$$\upsilon_g = \frac{c}{2d\sin(\theta - \theta_s)}. \tag{2.4.2}$$

where m is the mode number, L_e the cavity length change, and θ_s the grating rotation. Now the challenge becomes to find a pivot point for the grating that minimizes the tuning difference between the grating feedback and external cavity length ($\upsilon_{grating} - \upsilon_{ext}$).

In literature multiple theoretical approaches exist to maximize the mode-hop free tuning range of an ECDL. Nilse and colleagues propose a clear way to find this optimal pivot point [30]. Drawback of their method is that a

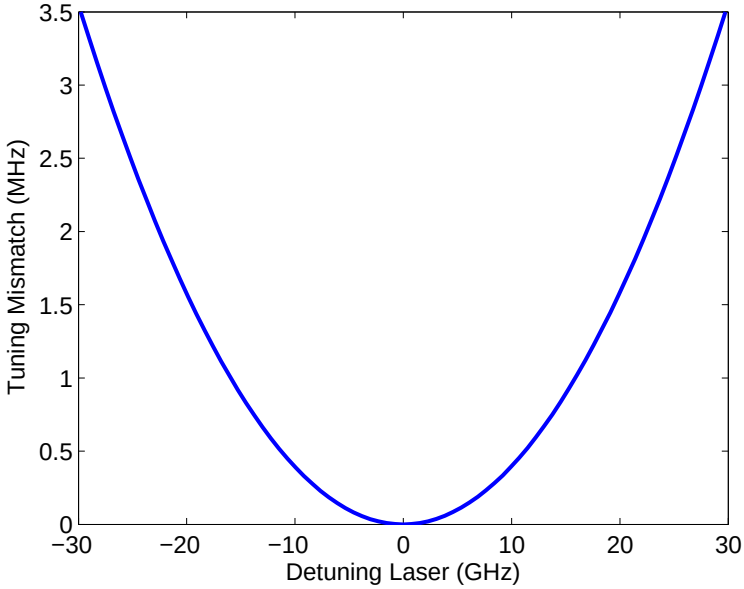

Figure 2.4.1: **Tuning mismatch.** Tuning mismatch between cavity length and optical feedback change originating from a rotation of the grating around the optimal pivot point.

slight offset of the actual pivot point has drastic consequences for the mode-hop free tuning range. Saliba and co-workers propose a different method were they search for the point were the location of the pivot point has the least influence [28]. Also, they fix the pivot point position and find the optimal cavity length. The ideal external cavity length is given by

$$L_{ideal} = L_g \frac{\tan\theta}{\cos\theta}, \tag{2.4.3}$$

where L_g is the distance of the pivot arm.

The theoretical tuning mismatch between the grating feedback and cavity length change ($\upsilon_{grating} - \upsilon_{ext}$) is plotted for varying detuning of the laser in Figure 2.4.1

Besides optimizing the geometry, the mode-hop free tuning range can be increased by a synchronous tuning the angle of the grating and the operating current of the diode. Since the output frequency of the ECDL is dependent on the operating current a feedforward from the driver that rotates the grating to the current can increase the mode-hop free tuning range.

Chapter 3

ECDL Design and Construction

During this project two ECDLs with operating wavelengths of 461 and 689 nm were built, which we will call the *blue* and *red* ECDL respectively. By choosing the grating pitch (and a bit of luck) the Littrow angle of the *blue* and *red* wavelengths is almost identical (∼56 degrees), i.e. within the tuning range of the grating mount. Therefore, after replacing the frequency dependent optical elements, the same design is used to construct an ECDL for both wavelengths.

We start this chapter by discussing the housing, optical, opto-mechanical, thermal, and electronic designs in Section 3.1. Next, we will discuss the construction of the ECDL, including optical alignment and rough wavelength tuning in Section 3.2.

3.1 Design

3.1.1 Housing

We use a massive aluminum laser housing with high heat capacity, which we decouple from the environment thermally and acoustically. The massive housing provides high stiffness and therefore mechanical resonances are suppressed. The grating is mounted on a standalone mount fixed on the housing. Therefore, various grating mounts can be implemented and the external cavity length can be varied. The housing is designed in SolidWorks and is milled out of a solid aluminum block by the University of Amsterdam Technical Workshop. The housing, including the lid, weights around 8 kg and is vacuum sealable. The complete ECDL design is shown in Figure 3.1.1.

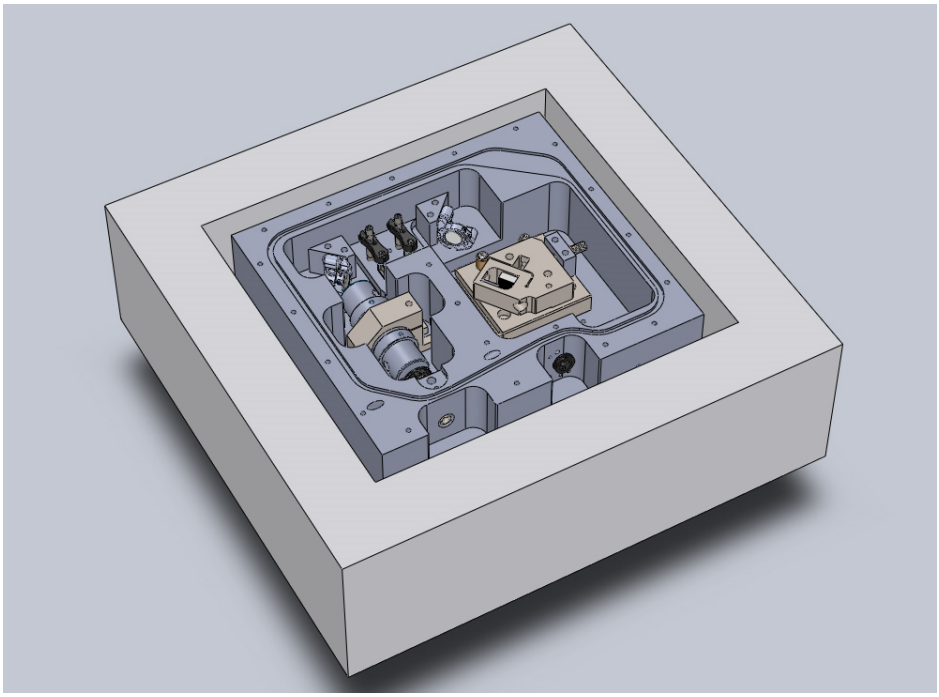

Figure 3.1.1: **Complete design ECDL.** The dimension of the grey aluminium housing is 240x220x70 mm. The outer white material represents the thermal insulation. The lid is not displayed.

	Blue	***Red***
Diode	Nichia NDB4216E	Opnext HL6738MG
Collimator	C330TMD-A	C330TMD-B
Collimation tube	LT230P-B	LT230P-B
Grating	GH13-36U	GH13-24V
Parallel mirror	ME05S-P01	
Isolator	Newport ISO-04-461-MP	IOT-5-670-VLP
Telescope	LK1753L1-A, LJ1402L1-A	LJ1402L1-B, LK1426L1-B
Mirrors	BB05-E02-10	
Mirror mounts	POLARIS-K05	

Table 3.1: **Items used in the *blue* and *red* ECDL.** Parts where no manufacturer is reported are purchased from Thorlabs.

3.1.2 Optical Configuration

The optical setup of the ECDL can be divided into three parts: the laser cavity (*Part A*), the optical isolation (*Part B*), and the fiber outcoupling (*Part C*), as illustrated in Figure 3.1.2. The part numbers of the items used for the *blue* and *red* ECDL are listed in Table 3.1. *Part A* is the heart of the ECDL and consist of a diode, collimator, and grating. The diode and collimator are mounted on a collimation tube, which is fixed to the massive housing (with one M3 screw) to provide stability and thermal conduction between diode and housing. The grating is placed under the Littrow angle (listed for the *blue* and *red* ECDL in Table 3.2), the grating mount designs are discussed in Section 3.1.3. The optical isolator in *Part B* protects against optical back reflections into the laser cavity that can cause instabilities and mode-hops. The fiber outcoupling is optimized by the elements of *Part C*. Due to the fiber coupling the ECDL can be decoupled from the environment. To fix the directional output beam while tuning, i.e. rotating the grating, a mirror parallel to the grating is added [25]. The cylindrical telescope transforms the elliptical beam into a (more) round beam by reducing the horizontal beam size by a factor of 40/15 (*blue*) or 40/25 (*red*). The two mirrors are needed to align the beam and the fiber coupler. The fiber coupler is mounted in the housing (with two M3 screws) to maximize stability. The fiber coupler can not be rotated and therefore a half-wave plate is added to achieve polarization maintained fiber coupling.

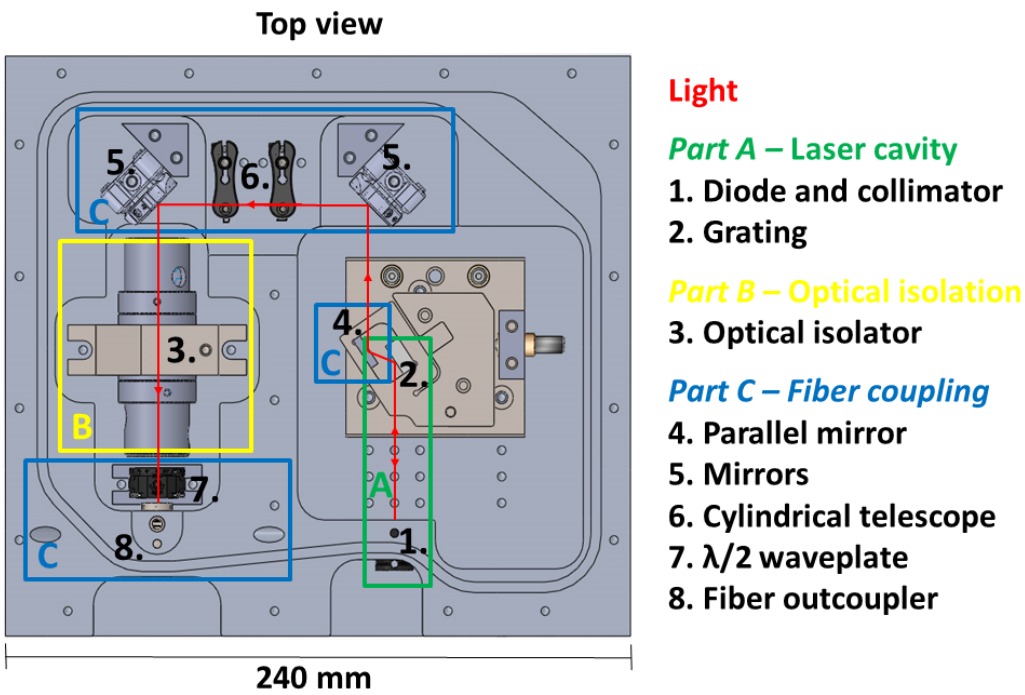

Figure 3.1.2: **Optical setup of the ECDL.**

		Blue	***Red***
Wavelength (nm)	λ	460.8626	689.4495
Grating pitch (mm)	d	1/3600	1/2400
Littrow angle (deg)	$\theta_{Littrow}$	55.77	56.05

Table 3.2: **Littrow angle for the *blue* and *red* ECDL.** The Littrow angle is calculated using Equation 2.2.2. Note that for both target wavelengths the Littrow angle is almost equal, i.e. within tuning range of the grating mount.

3.1.3 Opto-mechanical Configuration

The external cavity is the most challenging part to design for an ECDL. It is the most sensitive part since it forms the laser cavity and therefore should be maximally mechanical stable and maximally isolated. On the other hand, to frequency tune or lock the laser an opto-mechanical configuration is desired, which reduces the mechanical stability and limits the ability to isolate.

The grating mount needs to provide horizontal and vertical tuning, and, on top of that, additional horizontal fine-tuning via a piezoelectric actuator. Via the piezo the frequency of the laser can be tuned electronically even when the lid is closed. Absolute frequency stabilization can be achieved by providing frequency dependent feedback to the piezo. This so-called laser locking is discussed in Chapter 4 and 5.

Two sets of grating mounts are designed and fabricated: based on a commercial mirror mount (CMM) and based on a flexure in stainless steel. The CMM designs are simple, easy to manufacture, easy to align, and cheap. On the other hand, the stability is limited to the stability of the commercial mirror mount and the tuning is limited because there is not much space for a piezo. The flexure based designs are homebuilt and optimized for maximal stiffness and stability. Also, the flexure based designs should provide more tuning range compared to the CMM designs. Due to the limited duration of this master thesis there is not enough data to rigorously compare all designs. The data presented in this thesis is restricted to the flexure design.

Commercial Mirror Mount Design

A highly stable commercial mirror mount (Radiant Dyes MDI-HS) is used as the basis for the opto-mechanical tuning. The grating and parallel mirror are glued onto a homebuilt aluminum holder, which is screwed into the mirror mount. A piezoelectric actuator (Noliac NAC2012-A01) is glued onto the front plate at the location where the fine adjustment screw is supporting the front plate, as shown in Figure 3.1.4. The load is spread on the piezo by a

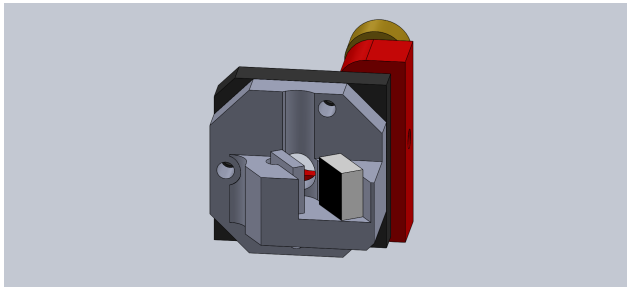

Figure 3.1.3: **Grating mount - Commercial mirror mount A.** The dimensions of the aluminum (gray) grating mount are 43.8x43.8x23 mm.

sapphire contact pad (Thorlabs P25SK2). The expected frequency tuning via the piezo is ∼5 GHz. Two almost identical designs for the aluminum holder exist; for short 17.6-57.6 mm (version A) and long 69.1-109.1 mm (version B) external cavity lengths. In version B the mirror mount is reversed to achieve longer external cavity lengths. All possible external cavity lengths are given in Table 3.3. The design of the CCM grating holder version A is shown in Figure 3.1.3.

Flexure Design

A flexure in stainless steel is used as the basis for the opto-mechanical tuning. This was a common and simple approach used in the first ECDL designs in the 1980s and is still used in the vast majority of both homebuilt and commercially available ECDLs. The mount is designed in SolidWorks and consists of two parts; a base and a top part, for vertical and horizontal alignment respectively. Simulations in SolidWorks were used to optimize the flexure designs. The complete flexure grating mount is shown in Figure 3.1.5.

The flexure for vertical alignment is designed as follows. The bottom of the baseplate is milled under 0.5 degrees, as indicated in Figure 3.1.6. When applying the maximum axial load capacity (6.8 kg each) on the two fine adjustment screws (100 TPI, Thorlabs Polaris P25SB100V) the flexure opens by 1 degree. This results in a vertical adjustment of ±0.5 degree with respect to the rear facet of the diode.

Horizontal alignment is divided into a rough and fine section. Rough horizontal alignment is achieved by rotating the top part over the base with a fine adjustment screw in combination with a dowel pin. The top part has two loose drill holes and is mounted on the base with two M4 screws. As a result the grating angle can be tuned to 56±1 degree with respect to the rear facet of the diode. Fine horizontal tuning is achieved via the flexure in

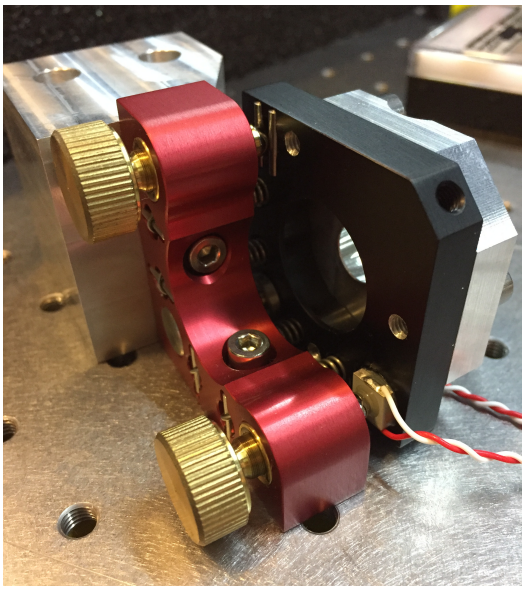

Figure 3.1.4: **Backside of the commercial mirror mount.** The 2 mm thick piezoelectric actuator (Noliac NAC2012-A01) is glued on the front plate of the commercial mirror mount (Radiant Dyes MDI-HS).

the top part in combination with a piezoelectric actuator. The theoretical tuning provided by the flexure is simulated with SolidWorks. Four versions of the top part exist and will be discussed in the next paragraph.

Four different versions of the top part were made, with a choice between greater stability or extra tuning, and a choice of external cavity length. The stability optimized version have a 11.0 mm piezoelectric stack actuator (Thorlabs PK4FA2P1) and an expected frequency tuning of 90 GHz. While the extra tuning versions have a 20.1 mm piezoelectric stack actuator (Thorlabs PK4FQP1) and an expected tuning of 290 GHz. The piezo is clamped into the top flexure with an M6 screw. The four grating holder versions were all fabricated, the designs are shown in Figure 3.1.7.

External Cavity Length

The external cavity length has a great impact on the linewidth of the ECDL, as explained in Section 2.2.3. However, instabilities due to temperature drifts imply a practical limit on the external cavity length for which stable lasing can be achieved. Therefore, we developed a design with a changeable cavity length. Possible external cavity lengths for the different grating mount designs are listed in Table 3.3. Also, for all grating mount designs the external cavity length to optimize the frequency tuning range is calculated (via

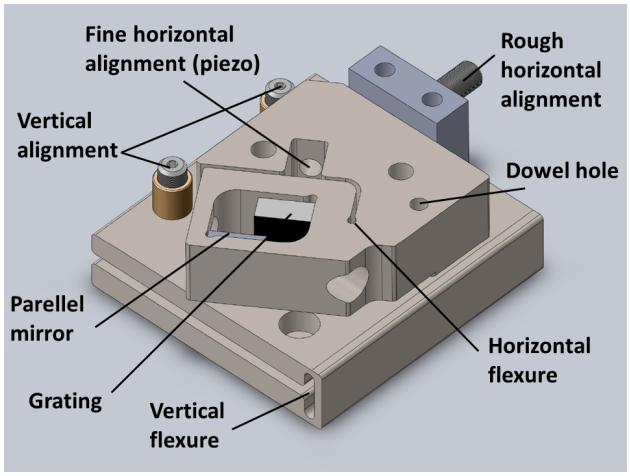

Figure 3.1.5: **Flexure design.** Flexure of stainless steel in combination with fine adjustment screws provide horizontal and vertical alignment. A piezoelectric acutator provides fine horizontal tuning.

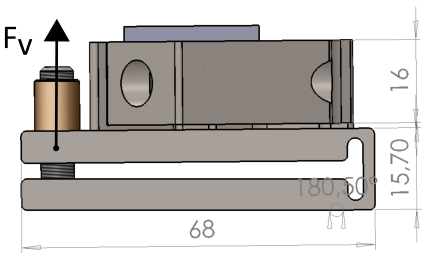

Figure 3.1.6: **Flexure design side view.** Two fine adjustment screws apply force F_v to the vertical flexure. Note that the moving part of the horizontal flexure (part including grating and parallel mirror) is floating 1 mm above the base. The used dimensions are mm.

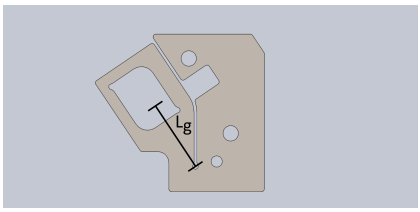

(a) Long arm - Stability

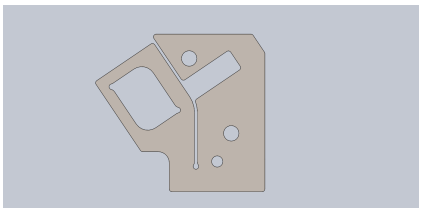

(b) Long arm - Tunability

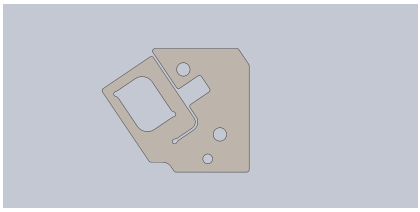

(c) Short arm - Stability

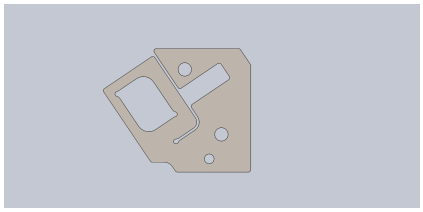

(d) Short arm - Tunability

Figure 3.1.7: **Four version of the flexure top part.** The arm is the distance between the pivot point of the flexure and the middle of the grating, as labeled by L_g in subfigure a.

Equation 2.2.2, as proposed by Saliba [28]) and listed in in Table 3.4.

3.1.4 Temperature Control

Both, the diode and external cavity must be temperature stabilized for stable single-mode lasing, as discussed in Section 2.3. Therefore the ECDL is temperature controlled passively and actively. Passive temperature control results from isolating the ECDL with 50 mm of polystyrene. For active temperature control a homebuilt temperature controller (TempPID v8.0, see Appendix A.2 for the circuit diagram) drives a cartridge heater (Sun Electric Heater H050-15-24-01) and a peltier (Adaptive Thermal Management ET-031-10-13).

Two temperature control elements are needed because we want to be able to have (fast) temperature control at a few mm from the diode, and we want to have a controlled link to the environment to extract or dump heat. The target temperature is set on the connector board of the ECDL, this board is discussed in subsection 3.1.5.

The active temperature control elements are configured as follows. The feedback for the temperature PIDs is received via NTC thermistors (TDK B57861S0103F40) that are placed as close as possible to the heating/cooling elements. The short feedback loops minimize temperature fluctuations [28]. A heatsink is attached to the peltier to dump/subtract heat to/from the

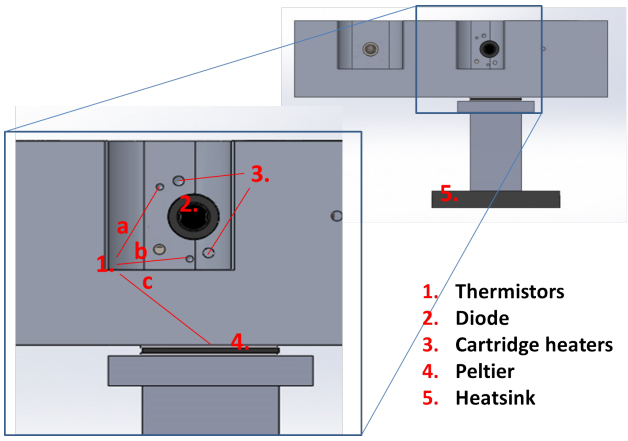

Figure 3.1.8: **Schematic of the active temperature control elements.** Front view of the ECDL housing. The cartridge heater and corresponding thermistor are mounted in *3a* and *1a* respectively.

environment. The position of the cartridge heater, peltier, thermistors, and heatsink is illustrated in Figure 3.1.8.

The temperature control settings are configured as follows. First, only the cartridge heater is used to temperature stabilize the diode at a temperature where stable single-mode lasing can be achieved at the target wavelength (30° Celsius for the *blue* ECDL, and 23° Celsius for the *red* ECDL). Next, the temperature PID setting of the cartridge heater are set to match the setting of the peltier PID. After testing the active temperature control the ECDL is thermally isolated.

Thermal Characterization

Since we use a massive aluminum housing and we only have a small amount of power in the temperature control elements, the temperature of the housing can only vary slowly in time. To find the time constant of this process we measure the temperature of the ECDL housing after a sudden switch-off of the diode. We expect that the temperature will first drop (since the diode produces heat) and later recover to the same temperature. During the measurement the housing is isolated and the temperature is measured at thermistor *1b*, as indicated in Figure 3.1.8. The measurement is plotted in Figure 3.1.9. Also, the data is fitted with an exponential fit and the corresponding exponential time constant equals $T_{crit} = 42$ minutes.

By temperature stabilizing the ECDL, the free running (not locked) frequency drift should be reduced. The *blue* ECDL is tuned to a single-mode stable region and its frequency is measured over 70 minutes with a waveme-

	P1	**P2**	**P3**	**P4**	**P5**	**P6**	**P7**	**P8**	**P9**	**P10**
Mirror Mount A	-	-	-	-	17.6	27.6	37.6	**47.6**	57.6	-
Mirror Mount B	-	-	**69.1**	79.1	89.1	99.1	109.1	-	-	-
Flexure Long Cavity	-	40.5	50.5	60.5	**70.5**	80.5	-	-	-	-
Flexure Short Cavity	-	**40.5**	50.5	60.5	70.5	80.5	-	-	-	-

Table 3.3: **External cavity lengths for different mounting positions.** The numbers in **bold** give the cavity length closest to the optimum.

	Arm L_g (mm)	**Angle (deg)**	**L_{ideal} (mm)**	**Tuning (GHz)**
Mirror Mount A	18.32	55.7714	47.86	5
Mirror Mount B	26.65	55.7714	69.63	5
Flexure Long Arm	25.93	55.7714	67.75	90 or 290
Flexure Short Arm	15.05	55.7714	39.32	90 or 290

Table 3.4: **External cavity lengths for optimal tunability.** The ideal cavity length L_{ideal} is calculated via Equation 2.4.3. Tuning is the theoretical tuning by maximum piezo displacement.

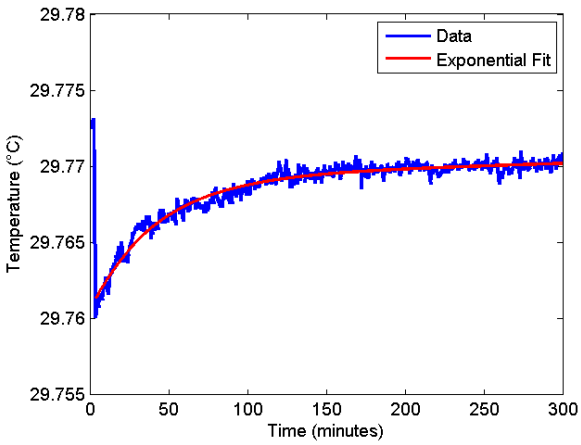

Figure 3.1.9: **Temperature of the *blue* ECDL after a sudden switch off of the diode.** The data (**blue**) is fitted (**red**) and the found T_{crit} equals 42 minutes.

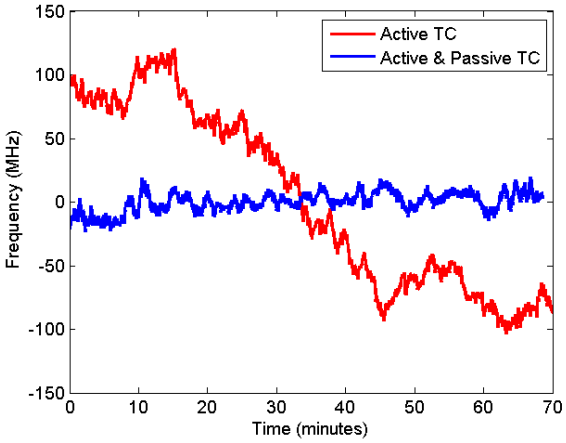

Figure 3.1.10: **Free running frequency drift of the *blue* ECDL.** The **red** curve represents the frequency drift of the output beam when the ECDL is only actively temperature controlled (TC). The **blue** curve represents the frequency drift of the output beam when the ECDL is actively and passively temperature controlled.

ter (High Finesse WSU). The average frequency over this time interval is subtracted and plotted in Figure 3.1.10. The free running frequency drift equals 200 MHz/h when the ECDL is only actively temperature stabilized. The free running frequency drift is reduced to 30 MHz/h when the ECDL is both passively and actively temperature stabilized. Note that stable lasing is not possible without active temperature control.

Since the ECDL is active temperature controlled for both curves in Figure 3.1.10 we can assume that the temporal behavior near the diode is similar. Therefore we can assume that the increase in frequency drift originates from external cavity length and grating angle changes due to temperature fluctuations in the external cavity.

3.1.5 Electronic Drivers

During the project multiple sets of electronics were used, including homebuilt and commercial modules. The current, temperature, and piezo modules were connected to the ECDL via a small circuit board, mounted on the outer box of the ECDL. The circuit diagrams of the homebuilt modules can be found in Appendix A.

***Blue* ECDL**	**Module**
Current driver	Toptica DCC110
Temperature control	Homebuilt (TempPID V8.0)
Piezo driver	Toptica SC110
PID	Toptica PID110

Table 3.5: **Electronical modules for the *blue* ECDL.** Circuit diagrams of the homebuilt modules are attached in Appendix A.

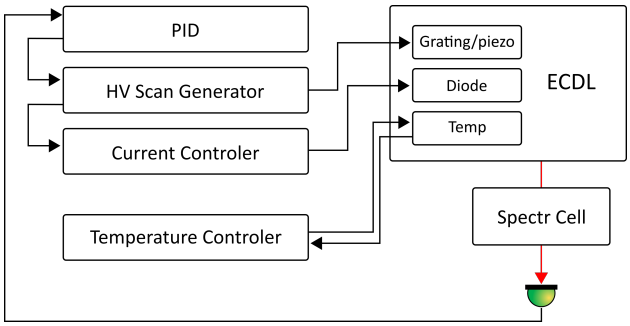

Figure 3.1.11: **Electronical setup for the *blue* ECDL.** The part numbers of the modules are listen in Table 3.5. The spectroscopy lock is discussed in Chapter 4.

Blue system

The connection diagram of the electronic modules of the *blue* laser system is illustrated in Figure 3.1.11, the corresponding part numbers are listed in Table 3.5. The piezo driver (DC 150V) has a feed-forward to the current controller to increase the mode-hope free tuning range, as discussed in Section 2.4. The temperature control system is discussed in Section 3.1.4. The absolute frequency stabilization with the PID via a spectroscopy lock is discussed in Chapter 4.

Red system

The connection diagram of the electronic modules of the *red* laser system is illustrated in Figure 3.1.12, the modules and corresponding part numbers are listed in Table 3.6. Since electronic noise can be the source of optical noise in the laser multiple current controller modules are tried. The homebuilt piezo driver (DC HV generator 150V) has no scan function. Therefore, an external function generator is used to perform an optical frequency scan via the piezo. The beat note lock is discussed in Chapter 5.

***Red* ECDL**	**Module**
Current driver	Homebuilt (LaserdiodeCD v6.0 500mA), Toptica DCC110, or Thorlabs LDC202
Temperature control	Homebuilt (TempPID v8.0)
Piezo driver	Homebuilt (HVDCDCWandler v2.0)
PID	Homebuilt (PID regulator v1.2 Jan 2006)
Function Generator	AIM-TTI TG550

Table 3.6: **Electronical modules for the *red* ECDL.** Circuit diagrams of the homebuilt modules are attached in Appendix A.

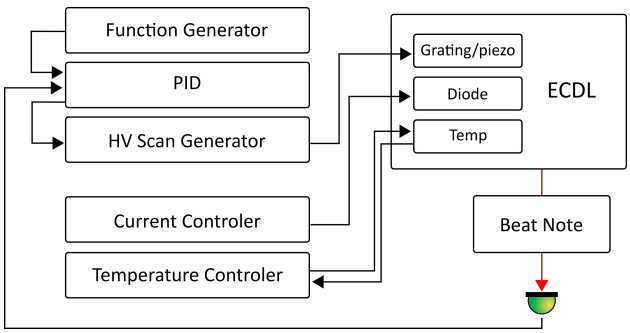

Figure 3.1.12: **Electronical setup for the *red* ECDL.** The part numbers of the modules are listen in Table 3.6. The beat note lock is discussed in Chapter 5.

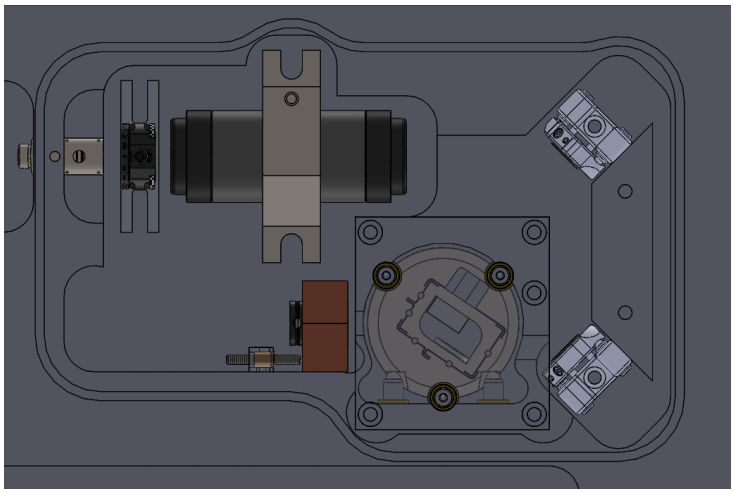

Figure 3.1.13: **Alternative flexure design.**

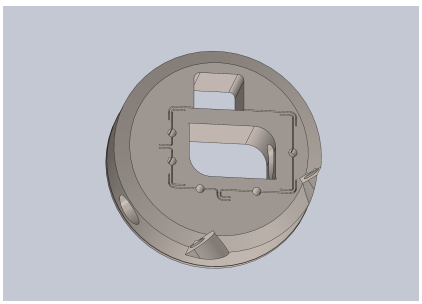

Figure 3.1.14: **Grating mount of the alternative flexure design.**

3.1.6 Alternative Flexure Design

Besides the approach we took, there are also other, more sophisticated, flexure designs. Early stage work is done to design a housing based on an approach by Kirilov and co-workers [31]. However, since this design is more complex we have chosen to focus on the simple design first.

In this alternative design, as shown in Figure 3.1.13, the degrees of freedom to align the diode and grating are different. Rough horizontal alignment is achieved via rotation of the total grating holder. Also, in contrast to our approach, the diode is not mounted at a fixed position. Therefore, vertical tuning is achieved by rotation of the diode and the cavity length can be varied by moving the diode. An advantage of this design is that the grating mount is more stable and rough horizontal (frequency) tuning can be achieved with a closed lid. The grating mount of this design is shown in Figure 3.1.14. The alternative flexure design has not been fabricated yet.

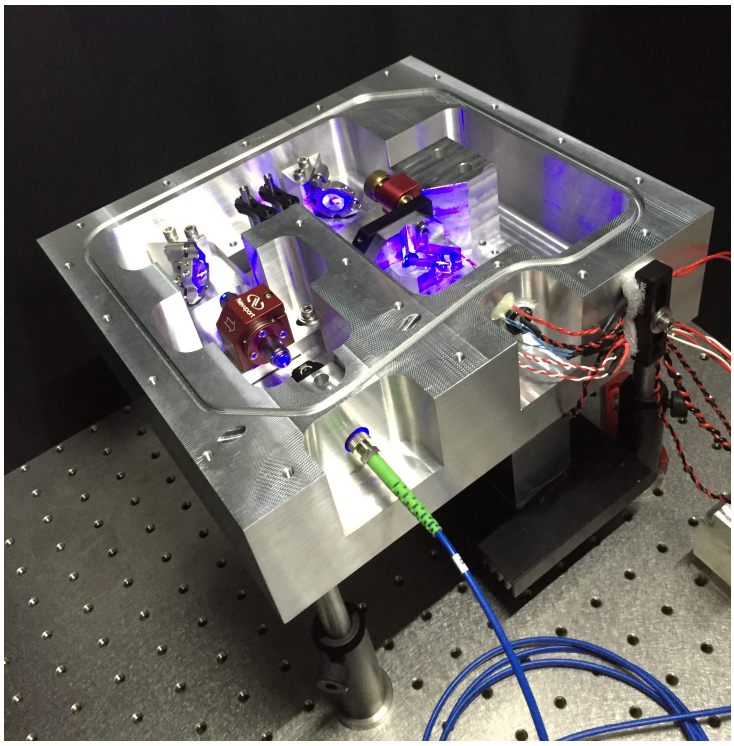

Figure 3.2.1: **Operating *blue* ECDL.** Configuration with the commercial mirror mount grating holder.

3.2 Construction

3.2.1 Optical Alignment

Optical alignment can be divided into three parts: diode, grating, isolator, and fiber couple alignment. Note that the part numbers of the optical elements are listed in Table 3.1.

Diode

The diode is rotated around the beam axis such that the long axis of the elliptical beam is parallel to the table plane. This maximizes the grating resolution (see Section 2.2.2) since the grating grooves are in the plane perpendicular to the table. Next, the beam is collimated with an aspherical lens. The beam is collimated by looking at the beam profile near the diode and at ∼2 m. The collimation lens is glued to the mounting tube, with two component epoxy glue, since there is some slack between the lens and the mounting tube.

Grating

Correct alignment of the optical feedback by the grating lowers the threshold current of the diode (see Section 2.1), this feature will be used to align the grating. First the grating is aligned so that the first order reflection is reflected back to the diode. Next, the current is set just below threshold. Now the grating is re-aligned so the diode starts lasing again. This is easily done by looking the at the blinking[1] output beam by eye, when moving the optics into and out of alignment. While repeating this steps the threshold for the blue laser diode is lowered from 30 to 25.5 mA. The steps are ~ 0.5 mA when starting optimization and lowered to ~ 0.1 mA when reaching the minimum treshold current.

Isolator

The isolator is optimized for a specific wavelength by reversing its direction and optimizing the isolation effect while rotating one of the polarizing beam splitters of the isolator. After the polarizing beam splitters are fixed in optimal position the isolator is reversed again, letting the laser diode beam propagate through it nearly unaffected, while blocking light propagating towards the laser diode. Next, the complete isolator is rotated to achieve maximal propagation of the beam. Since the operation efficiency of the isolator is wavelength dependent, the isolator is optimized after single-mode lasing at the target wavelength is achieved.

Fiber Coupling

The last step is coupling the beam into a fiber. Two low drift kinematic mirror mounts are used for optical alignment. A cylindrical telescope is used to transform the elliptical beam into a spherical one. The maximum fiber coupling efficiency for the blue and red ECDL are 55% and 65% respectivley. A weakness in the current design is that the telescope is positioned between the alignment mirrors of the fiber coupling. Therefore, the fiber coupling efficiency is very sensitive to the horizontal alignment of the mirrors.

3.2.2 Optimization of the Wavelength

As mentioned in Section 2.1, the center wavelength of the ECDL is affected by current, temperature, and grating angle.[2] For wavelength optimization

[1] Sudden increase of optical output power.

[2] Rule of thumb: higher current and/or temperature gives a larger wavelength, see Section 2.1.

	Blue	***Red***
Wavelength (nm)	460.8626	689.4495
Current (mA)	∼50	∼90
Temperature (°C)	∼ 30	∼ 23

Table 3.7: **Current and temperature settings to achieve lasing at the target wavelength.**

the output beam is monitored with a Fabry-Perot interferometer (homebuilt or Toptica FPI100) and a wavemeter (Burleigh WA-1500). The temperature and current settings for the target wavelengths are summarized in Table 3.7. Repeat the following steps for wavelength optimization:

1. Set the piezo to its middle position (75 V).
2. Minimize the threshold current of the diode by optimizing the vertical and horizontal alignment of the grating, as discussed in Section 3.2.1.
3. Specify a target current ($< 90\%$ of maximum current of the diode and in a large stable single-mode region).
4. Minimize the threshold current of the diode by optimizing the vertical alignment and tuning the temperature.
5. Set the current to its target value and achieve single-mode lasing by varying the current slightly.
6. Tune wavelength to its target value using the 'rough' horizontal alignment.
7. Repeat steps 4-6 until the threshold current is minimized at the target wavelength.

Chapter 4

Absolute Frequency Stabilization

For laser cooling, trapping, and probing of atoms the frequency stability of the laser is crucial. Frequency drifts of the laser, short- and long-term, should be smaller than the linewidth of the atomic transition they drive, <30 MHz for the 461 nm $^1S_0 \rightarrow {}^1P_1$ transition. Fluctuations in the environment are the main source for these drifts. With thermal control we can reduce some of these fluctuations, but we can never decouple the laser from its environment completely. Therefore we will lock the laser to an atomic transition in a gas of strontium.

In a gas at finite temperature the natural linewidth of an atomic transition is broadened by, amongst others, Doppler broadening obscuring the transition. To increase the locking resolution we introduce a pump and probe spectroscopy scheme. The theories behind Doppler-free saturated absorption and modulation transfer spectroscopy are summarized in Section 4.1 and 4.2 respectively. Next, the assembling procedure of the strontium spectroscopy cell is presented in Section 4.3. In Section 4.4 the experimental setup, optical and electrical, are discussed. The ECDL is frequency stabilized to the *blue* $^1S_0 \rightarrow {}^1P_1$ transition in strontium by a modulation transfer spectroscopy lock giving frequency feedback to the ECDL via a piezo, the results are discussed in Section 4.5. Finally, the locking procedure is listed in Section 4.6.

4.1 Doppler-free Saturated Absorption Spectroscopy

For a theoretical description of Doppler-free saturated absorption spectroscopy we follow the derivation by Foot [3]. We will approximate the internal en-

ergy level structure of the atom by a two-level system. For this system the absorption of a photon by an atom is illustrated in Figure 1.1.1.

Lets consider a laser beam with intensity $I(\omega)$, that travels through a cloud of atoms in the z-direction. The attenuation of the light equals

$$\frac{dI}{dz} = -(N_1 - N_2)\sigma(\omega)I(\omega), \tag{4.1.1}$$

where N_n equals the number of atoms per unit volume in state E_n, $\sigma(\omega)$ is the absorption cross section per atom and ω is the angular frequency of the light.

In the limit of high beam intensity the population in both levels becomes approximately equal ($N_1 \approx N_2$). By introducing $I_{sat}(\omega)$, the intensity for which the absorption transition becomes saturated and the transmission increases, and defining the total population $N = N_1 + N_2$, we can write the population difference as

$$N_1 - N_2 = \frac{N}{1 + I/I_{sat}(\omega)}. \tag{4.1.2}$$

By inserting equation 4.1.2 into equation 4.1.1 we get the following expression for the attenuation of a high power laser beam, $I(\omega) \gg I_{sat}(\omega)$, through a cloud of atoms

$$\frac{dI}{dz} = \frac{N\sigma(\omega)I(\omega)}{1 + I/I_{sat}(\omega)}. \tag{4.1.3}$$

In the equation above $\sigma(\omega)$ and $I_{sat}(\omega)$ vary with frequency. Rewriting the equation to show frequency dependence reveals that the line shape of the attenuation profile depends on intensity. This line broadening effect is called power broadening.

Now lets assume that an atom at rest absorbs radiation at ω_0, with natural linewidth Γ. The natural linewidth originates from the uncertainty principle relating the lifetime of an excited state with the uncertainty of its energy. However, moving atoms will experience a Doppler shift and will therefore absorb light at a shifted frequency. The radiation seen in the frame of the moving atom with velocity v equals

$$\omega' = \omega_0 - kv, \tag{4.1.4}$$

where $k = \omega/c = 2\pi/\lambda$, as illustrated in Figure 4.1.1.

For saturated absorption spectroscopy we introduce a second beam of low intensity, $I(\omega) < I_{sat}$, that counter propagates the high intensity beam. Due to the Doppler shift the so called pump ($I(\omega') \gg I_{sat}$) and probe beam

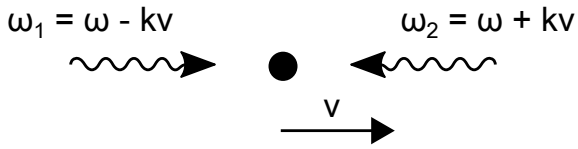

Figure 4.1.1: **Doppler effect.** Radiation frequency shift from actual frequency ω, to observed frequency ω_n, for a particle moving with velocity v.

$(I(\omega') < I_{sat})$ will address atoms of different velocity classes. However, both beams will be resonant with atoms that are not moving in the z-direction. The high intensity pump beam will saturated this transition and therefore bleach the atoms in this velocity class for the probe beam. As a result of this optical hole burning we will see a transmission peak with the natural linewidth of the probe beam.

4.2 Modulation Transfer Spectroscopy

Similar to Doppler-free saturated absorption spectroscopy, modulation transfer spectroscopy is based on a technique using two beams. Again, the beams are collinear, have opposite direction, and travel through a gas of atoms. Consequently a Doppler-free signal arises. Note that we will stick to naming the beams pump and probe; however, in this technique both beams will have approximately equal intensities.

Now, the key idea is to modulate the pump beam and observe the transfer of this modulation to the probe beam [32, 33]. Since the transfer is only efficient at (two-level) atomic resonances, they can be easily identified. Also, this results in a zero background signal, an advantage compared to other spectroscopy techniques that suffer from linear-absorption effects on the Doppler scale.

The transfer process is an example of four-wave mixing and originates from non-linear effects in the absorber [32]. The process is illustrated in Figure 4.2.1 for an atomic resonance ω_0, pump and probe frequencies ω, and a δ modulation of the pump beam. The modulated and original pump beam will combine with the probe beam. Resulting in a fourth wave: a modulated probe. After the modulation transfer, the original and modulated probe beam will interfere. The resulting beat signal can be observed with a photodiode and is given by [34]:

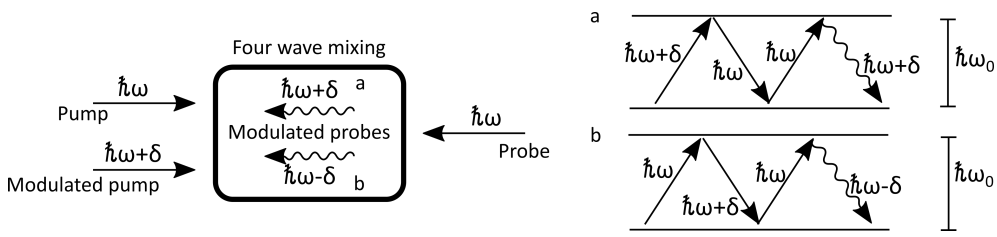

Figure 4.2.1: **Four wave mixing.** Modulation of the probe beam via four wave mixing. Note that in the experiment there are two modulated pump beams ($\hbar\omega \pm \delta$). *This figure is based on figures in reference [32].*

$$
\begin{aligned}
S(\delta) = \frac{C}{\sqrt{\Gamma^2+\delta}} \sum_{n=-\infty}^{\infty} J_n(\gamma) J_{n-1}(\gamma) \\
\times[(L_{(n+1)/2} + L_{(n-2)/2}) \cos(\delta t + \phi) \\
+(D_{(n+1)/2} + D_{(n-2)/2}) \sin(\delta t + \phi)],
\end{aligned}
\tag{4.2.1}
$$

where

$$
L_n = \frac{\Gamma^2}{\Gamma^2 + (\Delta - n\delta)^2}, \tag{4.2.2}
$$

and

$$
D_n = \frac{\Gamma(\Delta - n\delta)}{\Gamma^2 + (\Delta - n\delta)^2}, \tag{4.2.3}
$$

where we define $\Delta = \omega - \omega_0$ and J_n is the nth order Bessel function. Using equation above we can calculate the expected error signal.

4.3 Assembling the Spectroscopy Cell

To frequency stabilize the *blue* ECDL a strontium vapor cell is needed. A large vapor pressure is needed to achieve enough absorption for a clear locking signal. This poses a challenge since high temperature strontium atoms easily attach to the room temperature windows of the spectroscopy cell, making them less transparent. To overcome this problem two steps are taken. First, 10^{-3} mbar of argon, a noble gas, is added as buffer to keep the strontium gas away from the windows. Secondly, the solid angle from the strontium gas to the windows is reduced by placing the metalic strontium in a basket in the middle of a long (600 mm) and narrow (8 mm diameter) pipe. Due to

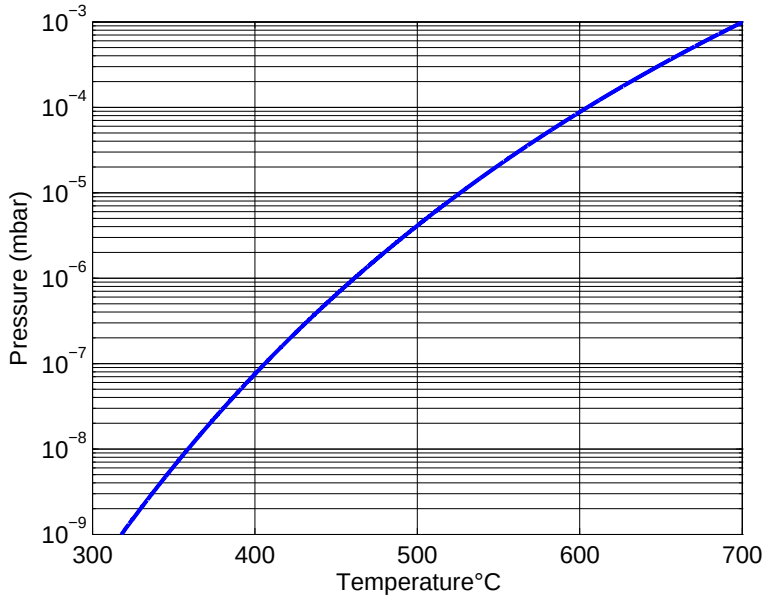

Figure 4.3.1: **Strontium gas pressure *vs.* temperature.**

this geometry the strontium basket in the center of the pipe can be isolated (multiple layers of glasswool, see Figure 4.4.4) and heated to 359° Celsius, while the windows are water cooled at room temperature. The spectroscopy cell is designed by Simon Stellmer, further details and design considerations can be found in Appendix A of his PhD thesis [35].

For a clean and (long-term) stable spectroscopy signal, the only gases substantially present in the cell must be strontium and argon. To achieve this we need to start with high quality vacuum. Lets first discuss the baking process to get there. Two one-meter heating bands were used to heat the cell, and twelve thermistors were placed at various places on the cell, valve, flanges, and turbopump to monitor the temperature. To realize high quality vacuum, two baking stages are required to remove all dirt. First, the cell is baked at 400° Celsius with the flanges attached. The heating from, and cooling to, room temperature takes roughly one day each. This results in a total bake time of four days. Secondly, we replace the flanges by windows and the cell is baked at 250° Celsius for one day. For this bake, with windows, even more care should be taken to minimize temperature gradients. Again, the heating from, and cooling to, room temperature takes roughly one day each. Before and during the bakes the cell is vacuum pumped, after the bakes the cell is leak tested with helium and a SRS RGA100 residual gas analyzer. In Figure 4.3.2 and 4.3.3 photographs of the spectroscopy cell are shown

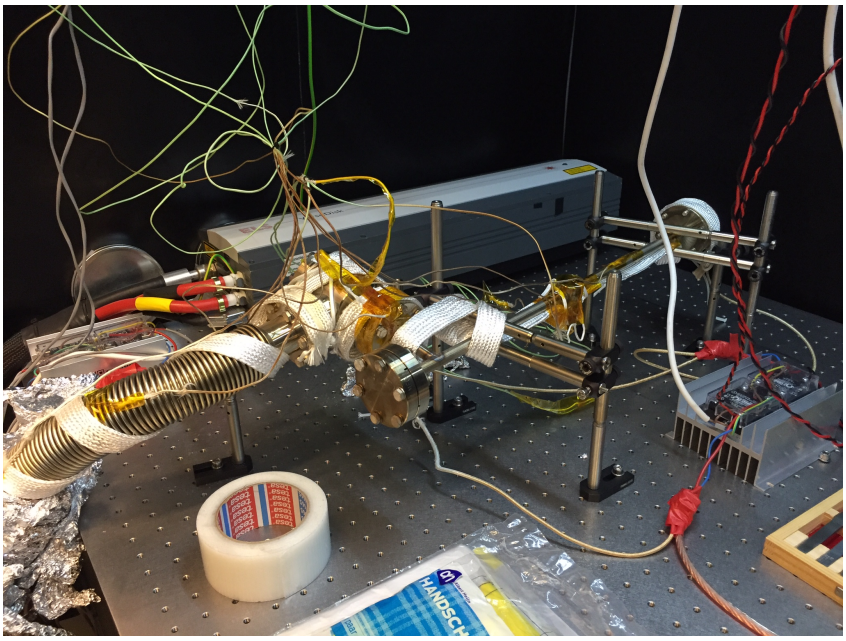

Figure 4.3.2: **Spectroscopy cell before the first bake**. Heating bands (white) and thermistors (green) are attached for temperature control during the bakes. Note that the windows are not attached yet.

before the first bake and during the second bake respectively. To check if the bakes cleaned the cell a mass scan is performed, the result is given in Figure 4.3.4.

After the baking process we can insert the strontium in the basket in the middle of the spectroscopy cell. Because strontium reacts with oxygen rapidly this process is time limited. To give ourselves more time we made a glove-box around the opening of the cell, as shown in Figure 4.3.5. Also, we create an overpressure inside the spectroscopy cell by flowing argon in via the vacuum pump. The entire process of inserting ∼7 gram of strontium took approximately 1 hour. The improvised glove-box did its job, however, it delayed the process because it was not completely transparent.

4.4 Experimental Setup

A schematic of the optical and electronical setup for the modulation transfer spectroscopy lock is given in Figure 4.4.1. A complete overview of the electronics used for the ECDL, including current control, temperature control, high voltage piezo driver, PID, and feedback loops was given in Section 3.1.5.

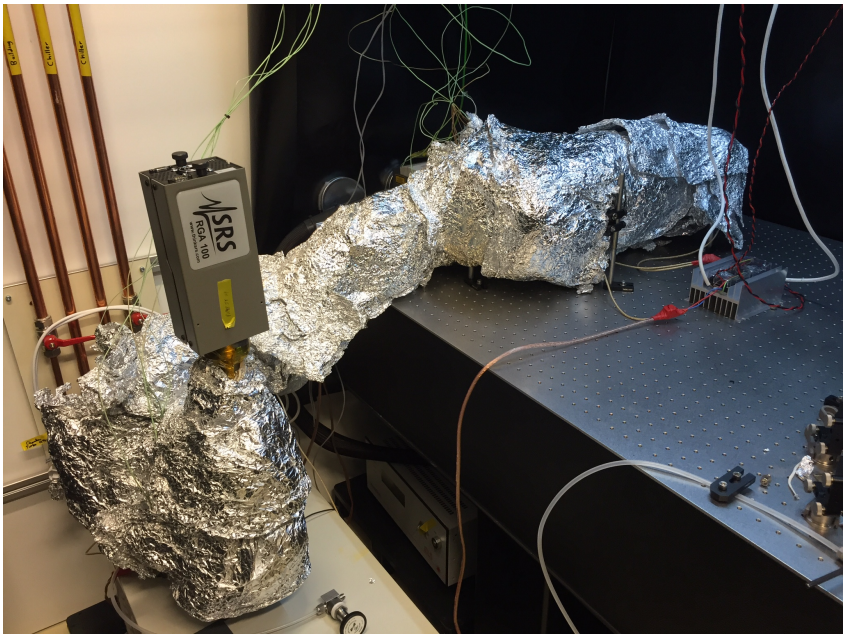

Figure 4.3.3: **Spectroscopy cell during the second bake.** During the bakes the cell and vacuum pump are isolated with multiple layers of aluminum foil.

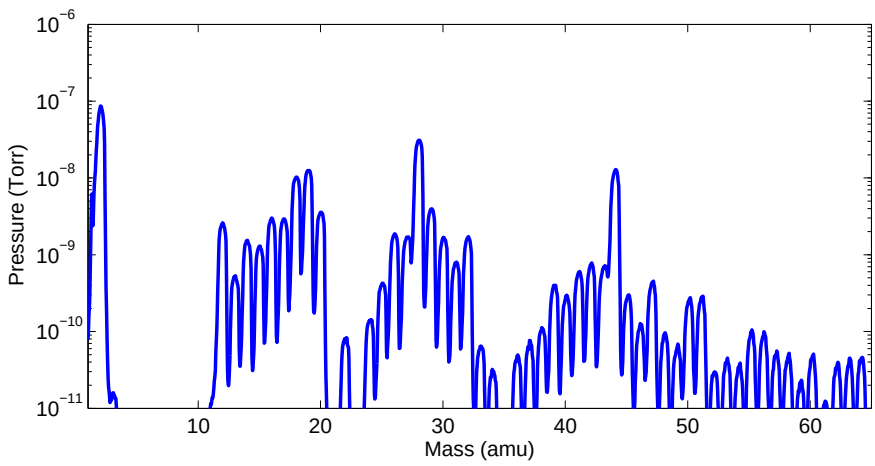

Figure 4.3.4: **Mass scan spectroscopy cell after pumping.** The pressure inside the spectroscopy cell for the first 65 amu, after pumping, after the second bake.

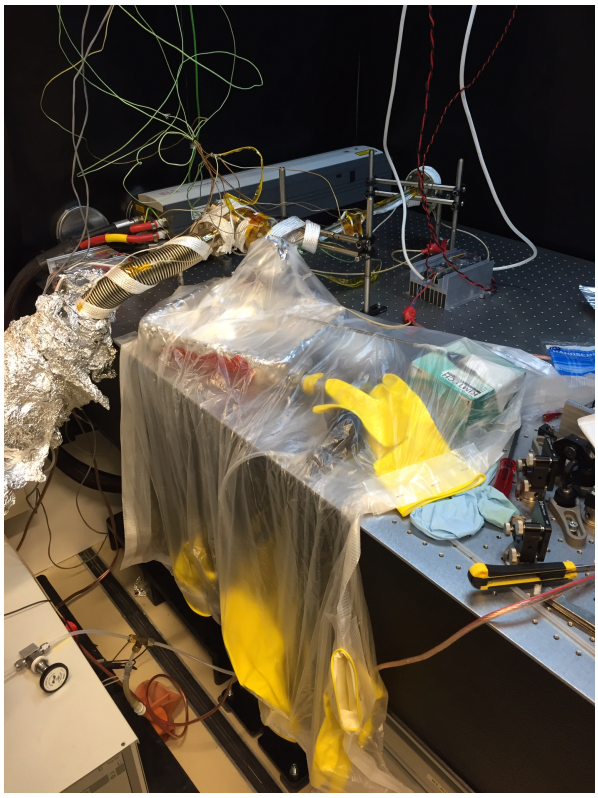

Figure 4.3.5: **Spectroscopy cell with glove-box.** To prevent strontium from reacting with oxygen while inserting in the cell a glove-box is made. Also, overpressure is created in the cell by flowing argon in via the vacuum pump.

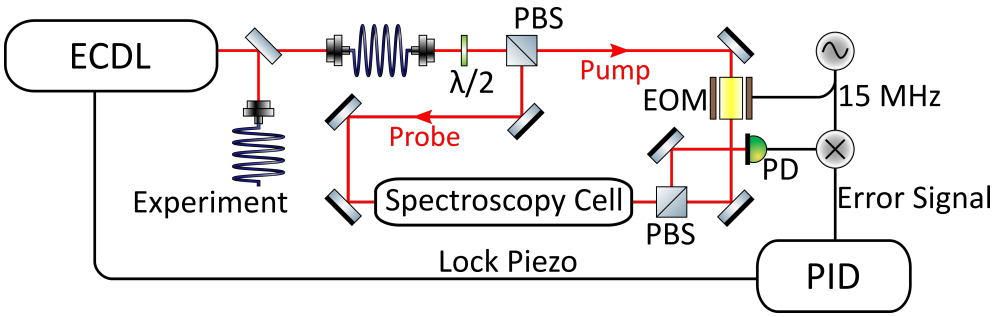

Figure 4.4.1: **Experimental setup for absolute frequency stabilization via modulation transfer spectroscopy.**

Again, we name our beams pump and probe, however, the intensities of both beams is almost equal. Both beams have a $1/e^2$ diameter of 0.5 mm and intensities of ∼1.5 mW.

Pump beam ω is modulated by an electro-optical modulator (EOM) with a frequency of $\delta = 15$ MHz. The EOM is homebuilt, the resonance frequency equals 15.094 MHz and a measurement of this frequency is shown in Figure 4.4.2. Sidebands of order n are formed at frequencies $\omega \pm n\delta$ and observed with a Fabry-Pérot interferometer, as plotted in Figure 4.4.3. The power ratio between the original signal and sidebands can be tuned by changing the radiofrequency power sent to the EOM.

Before we try to obtain the modulation transfer error signal, we start searching for the easy to find Doppler-broadened absorption signal. This is done by: aligning the probe beam through the cell on a photodiode, tuning the ECDL to the transition of interest ($^1S_0 \rightarrow {}^1P_1$, 460.8626 nm), letting the laser scan over ∼1 GHz, and looking at the signal of the photodiode on an oscilloscope. After we found the Doppler broadened (∼ 500 MHz) absorption dip we can start looking for the Doppler-free peak by introducing the pump beam. After aligning the pump beam properly a feature should arise at the bottom of the regular absorption peak, called the Lamb dip, as illustrated in Figure 4.5.1.

After observing the Doppler-free peak, we can expand our setup to create the dispersive error signal. We start modulating the pump beam via the EOM and mix-down (MiniCircuits ZP-3+) the AC coupled photodiode (bandwidth of 25 MHz) signal of the probe beam with the modulation frequency of the EOM. As a result, a dispersive DC error signal arises. By varying the phase delay (i.e. changing the cable length between the two arms before mixing) we can optimize the signal.

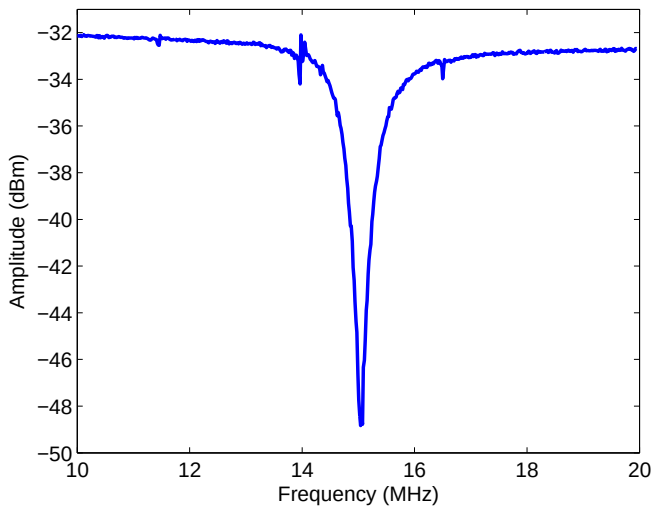

Figure 4.4.2: **Resonance frequency EOM.** The resonance frequency of the EOM is determined by measuring the reflectance of a signal by the EOM. The EOM has a resonance frequency at 15.094 MHz.

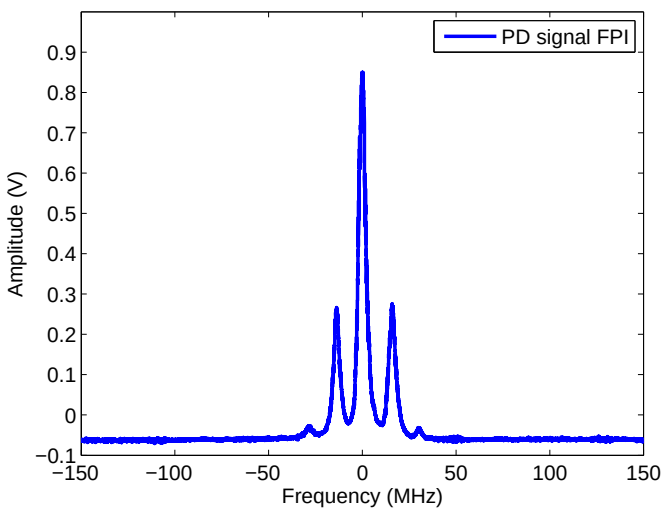

Figure 4.4.3: **Frequency modulation of pump beam.** Fabry-Pérot interferometer signal of the pump beam after modulation by the EOM. Two first order sidebands are visible at ±15 MHz form the center frequency. The amount of optical power in the sidebands can be tuned by changing the amount of power in the EOM.

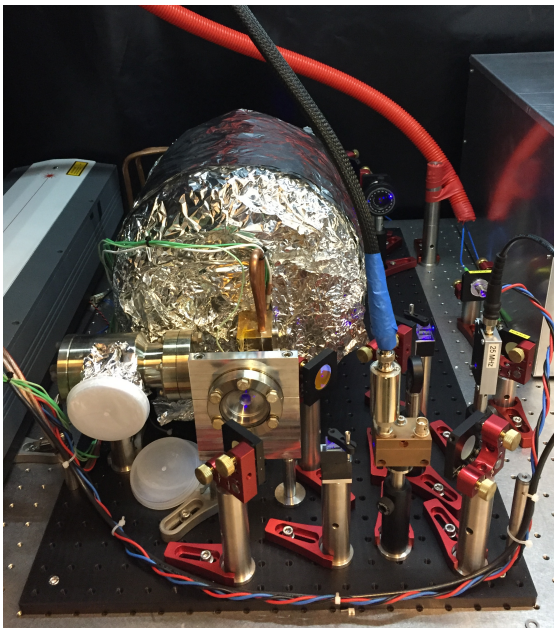

Figure 4.4.4: **Complete optical setup for absolute frequency stabilization.** The 'basket' with strontium is isolated with glasswool, the glasswool is covered with aluminum foil to keep the optical table clean.

4.5 Results

The *blue* ECDL is frequency stabilized to the 461 nm $^1S_0 \rightarrow {}^1P_1$ transition of strontium. The obtained Doppler-free peak in the absorption signal over a frequency scan of the laser is plotted in Figure 4.5.2. The corresponding peak-to-peak error signal is 30 mV and is plotted in Figure 4.5.1. During data acquisition the noise of the error significantly increased (possibly due to a ground loop), the actual signal to noise ratio is at least a factor of 2 higher. While taking data the pump and probe beams had powers of 1.2 mW each. The ECDL stays in lock for >1 day.[1]

4.5.1 Recommendations to Increase Error Signal

To increase the signal to noise ratio two approaches should be considered. One is increasing the beam size of both the pump and probe beam. The maximum beam size is limited by the diameter of the spectroscopy cell, however, it is not at its limit yet. The second is increasing the modulation

[1]The robustness of the ECDL design and the quality of the lock was demonstrated when a post-doc with a hammer showed up.

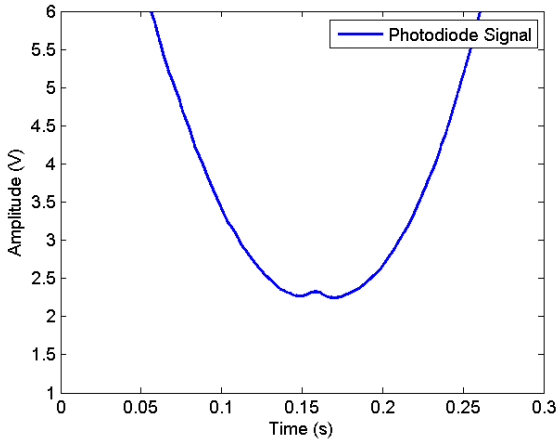

Figure 4.5.1: **Doppler-free peak.** Absorption signal for a frequency scan over $\sim$ 500 MHz of the *blue* ECDL.

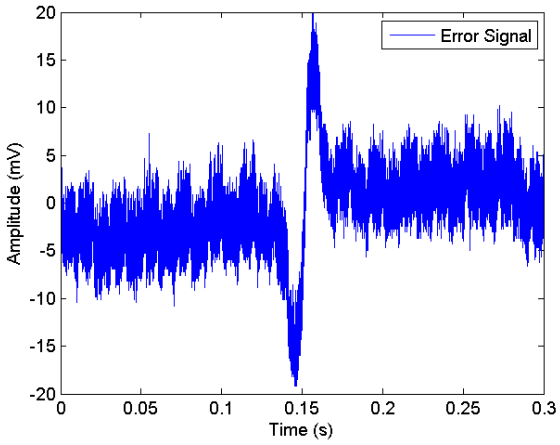

Figure 4.5.2: **Error signal modulation transfer spectroscopy.** Error signal for a frequency scan of the ECDL. Note that the error signal is not completely optimized.

frequency more towards the linewidth of the transition (30.5 MHz). Theory shows that we should expect an increased signal [33].

4.6 Locking Procedure

The locking procedure when locking the ECDL for the first time is as follows:

1. Completely lower (counterclockwise) the P, I and D settings on the PID.
2. Tune ECDL to 460.8626 nm (see Section 3.2.2).
3. Let laser scan over ∼1 GHz.
4. Observe error signal
5. Decrease scanning range, while keeping the error signal at the center of the scan.
6. Stop scanning
7. Find zero crossing of error signal by manually changing voltage on piezo.
8. Turn on the lock on the PID
9. Increase I such that the error signal is minimized
10. Increase P such that the error signal is minimized
11. Increase D such that the error signal is minimized

Chapter 5

Linewidth and Phase Noise Spectrum

Linewidth is one of the key parameters that characterize a laser, it quantifies the spectral purity of the light (i.e. frequency noise). Unfortunately, when the laser linewidth narrows the linewidth measurement becomes more complex. Center frequency drifts of the order of the linewidth at measurement time-scales will broaden the measured linewidth. Hence, frequency stabilization of the laser frequency is desired to make the linewidth measurements reliable. On the other hand, when a laser is frequency stabilized (locked), this will narrow its linewidth. Therefore, while measuring the linewidth of a laser one indirectly measures the lock performance. To start with, we want to characterize our laser and not the lock. For this reason we will use a slow (<100 Hz) lock. Also, we will try to reveal the origin of the linewidth broadening. In other words; we will decompose the noise in its frequency components, and, with this information, determine the noise sources.

This chapter is organized as follows. We start discussing noise in general by giving a frequency and time-domain representation in Section 5.1, followed by discussing different types of noise in Section 5.2. Next, we will discuss different measurement techniques to determine the phase noise or linewidth of a laser in Section 5.3, followed by an description of the experimental setup used to produce a heterodyne beat note in Section 5.4. In Section 5.5 the high frequency linewidth measurements are presented. Next, we will give the methodology and results of the power spectral density (PSD) measurements in Section 5.6. In this section we will also give a relationship between the PSD and the linewidth of a laser. The Matlab code to perform the PSD measurements is given in Appendix B.

5.1 Noise in the Time and Frequency Domain

To start with, we will briefly discuss noise in general. A more rigorous discussion can be found in reference [36]. When a signal is measured a distinction can be made between the (time-varying) signal S(t) and the noise N(t). Mathematically, the measured quantity V(t) is given by

$$V(t) = S(t) + N(t) = V_0 + \Delta V(t). \tag{5.1.1}$$

Assuming S(t) is constant in time it is convenient to use the definition as stated in the right equality of the equation above, including a constant term and a noise term varying in time.

The noise power is given by the variance of N(t) and is defined as

$$var(N) \equiv N_{rms}^2 \equiv \langle N(t)^2 \rangle. \tag{5.1.2}$$

In the time-domain the time-dependence of the noise can be obtained by computing the autocorrelation function of the noise term

$$R_N(\tau) = \langle N(t)N(t+\tau) \rangle. \tag{5.1.3}$$

However, it is more convenient to work in the frequency domain while discussing the time-dependency of a noise signal. Therefore, we define the noise spectral density $S_N(f)$ as the variance of the noise divided by the measurement bandwidth. This results in the following expression

$$S_N(f) = \frac{N_{rms}^2}{\text{measurement bandwidth}}, \tag{5.1.4}$$

having dimensions [V^2/Hz].

The time-dependence of the noise in the time and frequency domain, given in equation 5.1.3 and 5.1.4 respectively, are related via the Wiener-Khintchine theorem [37]. This is a special case of the Fourier transform where the Fourier transform is applied to the autocorrelation function of the signal instead to the signal itself. This is required since the noise signal, in contrast to the autocorrelation function, does not have a specified start and end. The transformation is given by

$$R_N(\tau) = \int_0^\infty S_N(f) e^{-i2\pi f\tau} df, \tag{5.1.5}$$

$$S_N(f) = 4\int_0^\infty R_N(f) e^{-i2\pi f\tau} d\tau. \tag{5.1.6}$$

Let us now consider the following (optical) signal:

$$V(t) = V_0 \ \sin[2\pi\upsilon_0 t + \phi(t)], \tag{5.1.7}$$

where υ_0 is the carrier frequency and $\phi(t)$ the phase noise. We assume that there are no intensity fluctuations (i.e. no intensity noise). This assumption is valid since we use a balanced detection scheme as discussed in Subsection 5.3.3. With the following equations we can write the phase noise as frequency noise and vice versa

$$\delta\upsilon = \frac{1}{2\pi}\frac{d\delta\phi}{dt}, \qquad \text{and therefore} \qquad \phi(t) = \phi_0 + \delta\phi(t) = 2\pi\delta\upsilon t. \tag{5.1.8}$$

Following equation 5.1.4 the frequency noise spectral density $S_{\delta\upsilon}(f)$, one-sided and with dimensions hertz squared per hertz, is now defined as follows

$$S_{\delta\upsilon}(f) = \frac{\delta\upsilon_{rms}^2}{\text{bandwidth used in measurement}}. \tag{5.1.9}$$

A complete derivation can be found in reference [38].

5.2 Types of Noise

Frequency noise can be divided into different classes, most commonly the following types are distinguished [36]:

- White noise
- 1/f noise
- Harmonic pertubations
- Drift

White noise is frequency independent and originates mostly from thermal and shot noise, which in their turn originate from thermal fluctuations and the quantization of nature respectively. In contrast, 1/f noise is inversely proportional to frequency and dominant at low frequencies only. It originates from impurities in the device (semiconductor material). Harmonic perturbations can be seen as pick-up from the environment at a specific frequency. While drift is a change in center frequency over a period greater than the experimental time scale, as illustrated in Figure 3.1.10. White and 1/f noise are plotted in Figure 5.2.1.

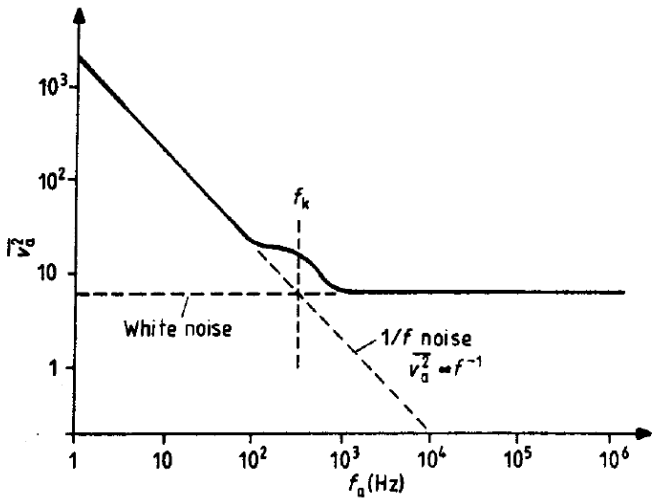

Figure 5.2.1: **Theoretical noise spectral density including white and 1/f noise.** *Figure is copied from reference [36].*

5.3 Linewidth Measurement Technique

5.3.1 Heterodyne Beat Note

To measure the laser linewidth (i.e. frequency noise) the heterodyne beat note technique is used [39]. The key concept of this technique is to lower the carrier frequency from optical (hundreds of THz) to radio ($\leq$MHz) frequency while not influencing the noise. As a result the optical noise can be measured with a photodiode. By interference with a second laser the carrier frequency of the original signal is lowered to $v_s - v_{LO}$, here v_{LO} is the center frequency of the reference laser (local oscillator) and v_s is the center frequency of the laser under test (signal). The beat note signal is described by [39]:

$$V(t) = R[P_{LO}(t)+P_s(t)+2\sqrt{P_{LO}(t)P_s(t)}\cos(2\pi(v_{LO}-v_s)t+\Delta\phi(t))], \quad (5.3.1)$$

where R is the photodiode responsivity, $P_{LO}(t)$ and $P_s(t)$ are the powers of the local oscillator and signal laser respectively, and $\Delta\phi(t)$ is the phase difference between the lasers. The photodiode bandwidth should be $BW_{PD} > v_s - v_{LO}$. This so called *frequency down-mixing* is illustrated in Figure 5.3.1.

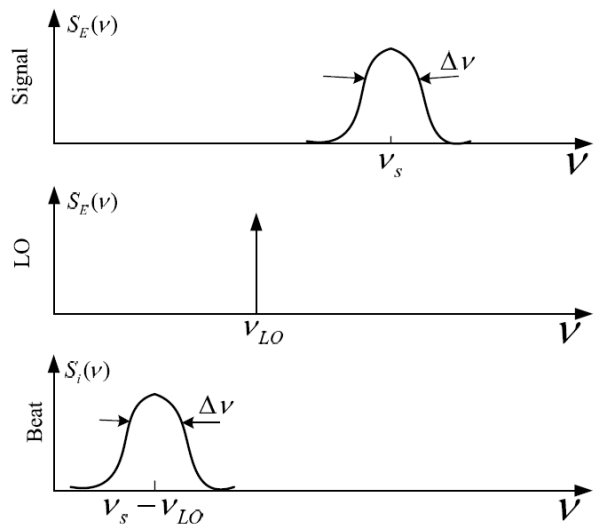

Figure 5.3.1: **Frequency down-mixing.** The upper plot represent the frequency distribution of the laser under test. In the middle plot we approximate the reference oscillator frequency spectrum by a delta function. The lower plot illustrates the beat note, containing only the noise of the signal laser at a frequency $v_s - v_{LO}$. *This is copied from reference [39]*

5.3.2 Reference Laser

The linewidth of the reference signal is a crucial parameter since the noise in the beat note is a combination of the two interfering signals. The reference source is a frequency stabilized Toptica DL100pro, locked to a homebuilt high finesse cavity, with an estimated linewidth of < 2 kHz [35]. Only a limited amount of light is available from the source laser. Therefore, an injection locked diode slave laser is used to make more power available. Via the slave laser 2 mW of power is used to produce the beat note. The effect on the linewidth induced by the slave laser is minimal.[1]

5.3.3 Balanced Detection

To cancel intensity noise two photodiodes (bandwidth of 1 GHz) in a balanced detection scheme are used [40, 41]. In absence of a 180° out of phase subtractor an adder in combination with a delay in one of the arms is used. To be able to tune the delay one of the photodiodes is mounted on a translation stage.

5.3.4 Alternative Linewidth Measurement Techniques

Alternative linewidth measurement techniques exist. By letting the laser interfere with itself one can create a beat note without a reference laser; which is a possible noise source. However, the interfering beams must be incoherent. For narrow-linewidth lasers this becomes impractical for a free-path delay and very expensive for a fiber based delay.[2] Alternatives are to build two identical lasers and let them interfere with each other or to use a cavity interferometer.

5.4 Experimental Setup

A setup has been built to measure the beat note between the ECDL and the reference laser. Figure 5.4.1 shows a schematic of the setup and Figure 5.4.2 shows a photograph of the optical part of the setup. Roughly 8 mW of ∼689 nm light of the ECDL is used as input power for the setup. The wavelength is precisely tuned by changing the optical-feedback given by the grating via

[1] In our ultracold strontium experiments injection-locked slave lasers are used to produce a stable strontium MOT on the 7.4 kHz red cooling transition. This gives reason to believe that the linewidth of the slave lasers is <7.4 kHz.

[2] When working with lasers at telecom wavelengths (1550 nm) optical fibers are much cheaper. Therefore, a fiber based delay is a neat and inexpensive approach.

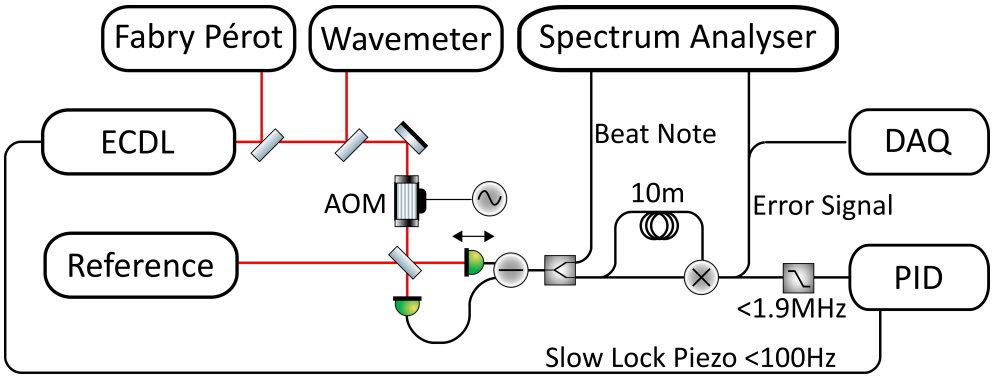

Figure 5.4.1: **Experimental setup to measure heterodyne beat note.** The red lines represent the light (optical part), and the black lines represent the wires (electrical part).

a piezo and changing the driving current of the diode, while monitoring the wavelength with a wavemeter (Burleigh WA-1500). To monitor whether the ECDL runs single mode a home-built Fabry-Perot interferometer is used. Also, the laser is temperature stabilized at 23° Celsius. For an overview of the ECDL setup, including current, temperature, and piezo drivers setup see Chapter 3. As mentioned in Section 5.3.3 two photodiodes with a 1 GHz bandwidth are used to convert the optical signal to an electrical signal. An AOM shifts the frequency of the ECDL by 80 MHz. This is not essential to produce the beat note, however, via the AOM we can introduce a known amount of frequency noise to the light. This gives us a possibility to calibrate the power spectral density measurements.

5.4.1 Beat Lock

As pointed out in the beginning of this chapter; frequency stabilization (locking) and laser linewidth are strongly related. To minimize the effect of the lock on the linewidth we will stabilize the laser frequency with a slow (<100 Hz) lock. The relation between the linewidth and lock is best explained by inspecting the PSD measurements, which is done in Section 5.6.3.

To frequency lock the ECDL the beat note is converted into a dispersive error signal which gives feedback on the laser frequency via the grating. The error signal is introduced by coupling out 1/10 of the beat note signal (Mini-Circuits ZDC-10-1), introduce a phase delay (10 m shielded BNC-cable), and mixing the signals back together (Mini-Circuits ZP-3). The signal is cleaned with a 1.9 MHz low-pass filter (Mini-Circuits BLP-1.9) before entering the home-built PID, a circuit diagram of the PID is given in Appendix A.3. A

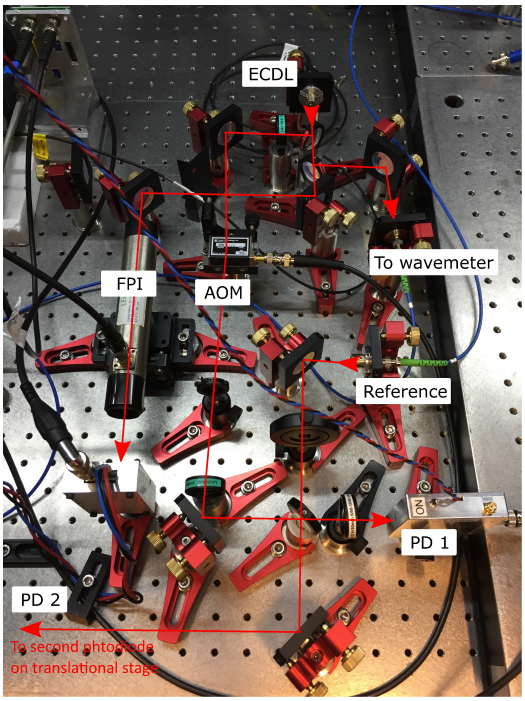

Figure 5.4.2: **Experimental setup to measure heterodyne beat note.**

schematic of the beat lock setup is given in Figure 5.4.1.

5.5 High Frequency Linewidth Measurement

To perform high frequency ($\sim$ 500 MHz) linewidth measurements the beat note signal is partly coupled out and analyzed by an electronic spectrum analyzer (Rohde & Schwarz FSH3). With the slow lock operational, the frequency spectrum of the beat note is measured and plotted in Figure 5.5.1, 50 sweep average with a 3 kHz resolution bandwidth (RBW). The dips around 320 and 630 MHz are due to balanced detection without proper subtractor.

To obtain a linewidth the trace is fitted to a Voigt profile, composed of a Gaussian and Lorentzian part, from which the full-width at half maximum (FWHM) is extracted. Experiments show that the frequency noise of a single-mode laser is characterized by white noise (Lorentzian profile) and 1/f noise (Gaussian profile) [42]. The Gaussian component contributes mainly to the peak, while the Lorentzian component has mainly contributes to the wings of the line shape. The Voigt fit is plotted in Figure 5.5.2. The fitted Gaussian, Lorentzian, and Voigt FWHM linewidths are listed in Table 5.1.

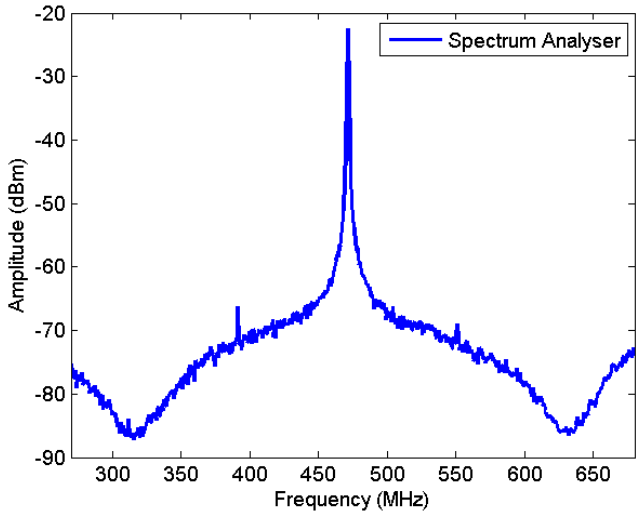

Figure 5.5.1: **High frequency spectrum beat note.** The dips at 315 and 635 MHz are due to the balanced detection without subtractor.

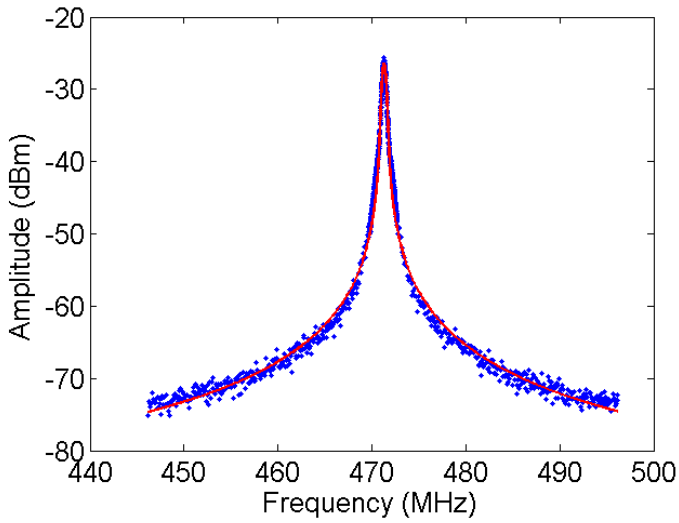

Figure 5.5.2: **Voigt fit of the high frequency spectrum.** Trace with: 30kHz RBW - 2.39s SWT - 50 times average.

Line Shape	**Linewidth$_{FWHM}$ (kHz)**
Voigt	443
Gaussian	384
Lorentzian	113

Table 5.1: **Fit results frequency spectrum linewidth.** The Voigt line shape has Gaussian and Lorentzian contributions. The Voigt fit is plotted in Figure 5.5.2

5.6 Low Frequency Linewidth Measurement

To have a second characterization method for the spectral purity of the ECDL, and, more importantly, reveal the origin of these impurities, we will further analyze the frequency noise. In other words, we will decompose the noise into its frequency components, and, with this information, determine the noise sources. Hence, we can conclude that the noise is fundamental, or, if it is not, make adjustments in the design to improve the spectral purity (i.e. reduce the linewidth) of the laser. Similarly, by looking at (the absence of) mechanical resonances, we can draw conclusions about the stiffness of our design.

By measuring the beat note signal, computing the autocorrelation, and performing the Fourier transformation we obtain the power spectral density (PSD). However, before we can get physical information out of the data we need to improve the signal to noise ratio and correctly scale our data.

5.6.1 Time Averaging the PSD

By time averaging random noise is filtered out, and, as a result, periodic noise is revealed that is otherwise buried in the random noise. First, the data is divided into time-windows and the autocorrelation functions and Fourier transforms are computed. Next, we average over the time-windows. Averaging of Fourier spectra via this method was introduced by Welch in 1967 [43].

For a PSD measurement there is a trade-off between resolution bandwidth and computation time. The bandwidth of the measurement is determined by 1/T, where T equals the measurement time of a window. The fast Fourier transform induces a computational limit on the number of data points for which we can compute the fast Fourier transform in a reasonable time. Taking the prior into account, each measurement consist of 80 seconds of data with a sampling rate of 10^6 s^{-1}. The data is divided into 39 parts of 4 seconds

each, as illustrated in Figure 5.6.1.

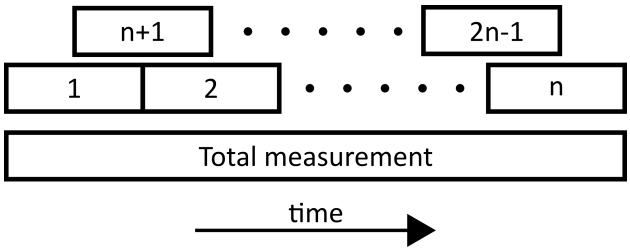

Figure 5.6.1: **Time-windows measurement.** The total measurement time is 80 s, the data sampling rate equals 10^6 s^{-1}, and n equals 20. In total we obtain 39 time-windows of 4 s.

5.6.2 Scaling the PSD

By adding a known amount of noise to the optical signal the PSD measurements can be scaled. The noise is added via an acoustic-optical modulator (AOM). In this way we leave the ECDL itself untouched and we can see this as a 'clean' way to add noise. The signal beam is first order diffracted by the AOM (+80 MHz). The driving frequency of the AOM is modulated with a peak-to-peak depth $\Delta\upsilon_0$ and frequency υ_M. Since $\upsilon_{rms} = \Delta\upsilon_0/\sqrt{2}$ we can rewrite equation 5.1.4 as

$$S_{\delta\upsilon}(f) = \frac{\Delta\upsilon_0^2/2}{\text{bandwidth used in measurement}}. \tag{5.6.1}$$

It is assumed that the scaling is linear over the measured Fourier frequency domain. In this way one calibration peak can be used to scale the complete measurement.

5.6.3 PSD Measurements

Experimentally, noise measurements are challenging because extra noise can arise from all kinds of sources in the system and its environment. In this research great effort is made to reduce additional noise. This is done in the following ways: cables are kept as short as possible[3], cables are shielded, grounding loops are avoided, differential signals and balanced detection are used.

[3]The location of data acquisition, and therefore the PC, is as close as possible to the optical setup.

Figure 5.6.2 shows a power spectral density plot of the frequency noise for four different measurements. In light blue the PSD is plotted for the ECDL including a slow lock (<100 Hz) on the piezo, while in dark blue the laser is not locked and therefor free-running. The plot clearly shows that the slow lock will suppress frequency noise below 100 Hz. The measurements given in purple and red are performed to define the electrical noise floor of the system.

The PSD of the locked ECDL (light blue) shows multiple resonance peaks in the range 90-2000 Hz. Since these peaks are also present in the detector noise measurement (purple) it is likely that the peaks are measurement noise.

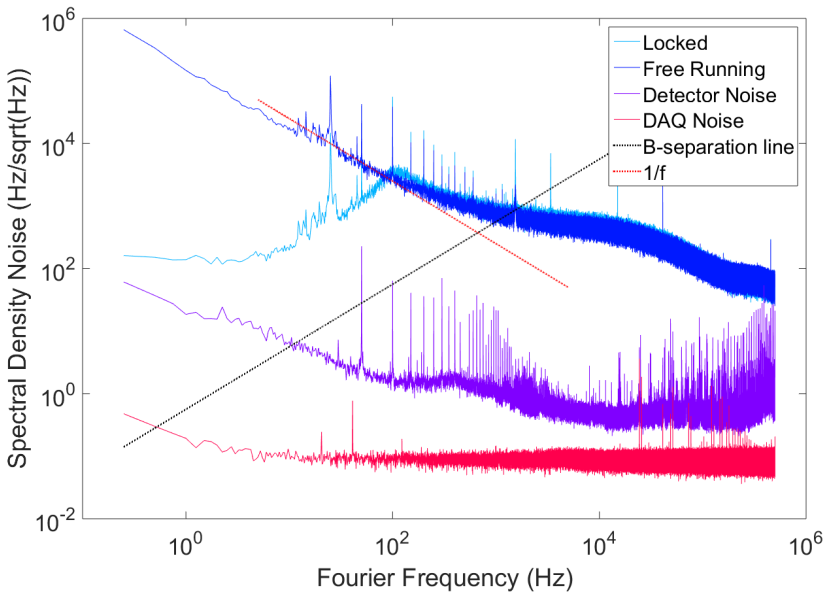

Figure 5.6.2: **PSD measurement.**

5.6.4 PSD to Linewidth

As expected, the PSD is related to the linewidth of a laser. However, this relationship is not straightforward and in literature various approaches that describe this relation exist. In this thesis we will follow the 'simple' approach proposed by Di Domenico and co-workers [44]. Applying this approach the data of the locked laser (light blue) of Figure 5.6.2 gives a Gaussian linewidth of 230 kHz.

The approach is based on the so-called β-separation line, where β is the modulation index of the noise and is defined as $\beta = 8\ln(2)f/\pi^2$. The pre-factor originates from the fact that we assume a Gaussian line shape. When

the power spectral density, $S_{\delta\upsilon}(f)$, is greater than this β-separation line it will contribute to the peak of the line shape (Gaussian part). When the noise is below the line it will contribute to the wings of the line shape (Lorentzian part) and is ignored. Intuitively this can be understood by modulation theory; when the noise level is high compared to the modulation frequency a deep and slow modulation will occur. In contrast, when we have a modulation with a low modulation index, the modulation will be too fast to have a significant effect on the linewidth, and will therefor only contribute to the wings. The Gaussian FWHM of the laser linewidth can now be estimated as follows

$$\Gamma_{FWHM} = (8\ln(2)A)^{1/2}, \tag{5.6.2}$$

where A is given by

$$A = \int_{1/T_0}^{\infty} H(S_{\delta\upsilon}(f) - 8\ln(2)f/\pi^2)S_{\delta\upsilon}(f)\mathrm{d}f, \tag{5.6.3}$$

and where H(x) is the Heaviside function.

5.7 Discussion

5.7.1 Sidebands Reference Laser

For heterodyne linewidth measurements it is crucial that the frequency noise in the reference laser is approximately zero (compared to the laser under test). However, spectroscopy measurements with the reference laser give reason to believe that it has sidebands at ±0.8 MHz with a significant amount of power. The measurements suggest that the reference laser has a Lorentzian line shape at frequencies beyond 1 MHz with an effective linewidth of the order of 200 kHz. This additional noise can explain the bad Voigt fit at ±0.8 MHz from the center frequency, as shown in Figure 5.7.1. If this is the case the linewidth measurements are affected and the found FWHM linewidths must be interpreted as upper limits. Further research concerning these sideband is needed. If it turns out that the sidebands are present, they should be suppressed and the linewidth measurements should be retaken.

5.7.2 Grating Mount Resonance Frequencies

Simulations with SolidWorks have been done to find the resonance frequencies of the flexure based grating mount, and the resonance modes of the top part are listed in Table 5.2, and, similarly, the resonance modes of the base are

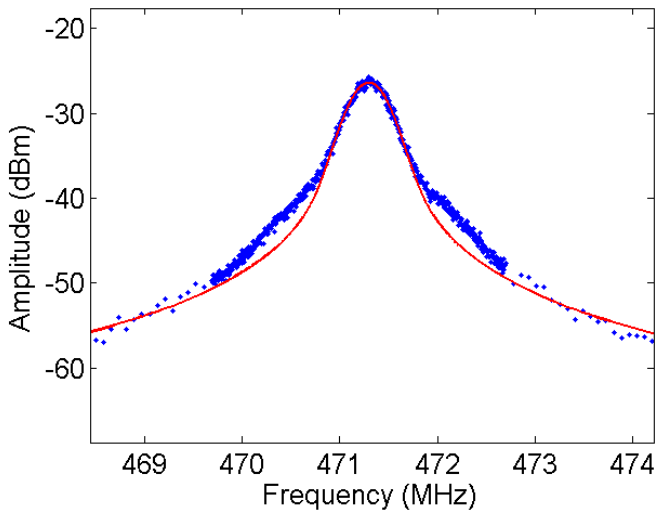

Figure 5.7.1: **Voigt fit of the high frequency spectrum.** Trace with: 3 kHz resolution bandwidth, 50 averages, and 50 MHz span.

Mode No.	Frequency(Rad/s)	Frequency (Hz)	Period (ms)
1	15553	2475.3	0.40399
2	20390	3245.2	0.30814
3	45497	7241	0.1381
4	55768	8875.7	0.11267
5	85986	13685	0.073073

Table 5.2: **Resonance frequencies top flexure grating mount.** Simulation of the on stability focused short cavity version.

listed in Table 5.3. In the PSD measurement of Figure 5.6.2 a resonance peak is visible at 1.7 kHz which probably corresponds to this resonance.

Mode No.	**Frequency(Rad/s)**	**Frequency (Hz)**	**Period (ms)**
1	1475	234.75	4.2598
2	5206.9	828.7	1.2067
3	10870	1730	0.57804
4	11093	1765.5	0.56642
5	29147	4639	0.21557

Table 5.3: **Resonance frequencies base flexure grating mount.**

Chapter 6

Summary and Outlook

6.1 Summary

An introduction to laser physics was given and the key properties of semiconductor lasers have been discussed. Also, a literature study has been conducted summarizing the state-of-the-art in ECDL design. Based on this knowledge two ECDLs were designed, built, frequency locked, and characterized: a *blue* and a *red* ECDL with wavelengths of 461 and 689 nm respectively.

An massive aluminum ECDL housing with an interchangeable grating mount was designed. Multiple grating mount designs were developed focusing on stability, tunability, or manufacturing ease.

After decoupling the *blue* ECDL from the environment acoustically and thermally the free-running center frequency drift was < 30 MHz/h. For absolute frequency stabilization a strontium spectroscopy cell was built. The *blue* ECDL was successfully locked to the $^1S_0 \rightarrow {}^1P_1$ transition in strontium with a modulation transfer spectroscopy lock and stayed locked for >1 day.

A heterodyne beat note setup was built and a beat note was measured between the *red* ECDL and a reference laser. The measured free-running FWHM linewidth was 397 kHz, while a Voight fit resulted in a FWHM of 443 kHz (Lorentzian 113 kHz + Gaussian 384 kHz). However, since the reference laser had a significant amount of noise, it influenced the measured linewidth of the beat note. Therefore, the values of the FWHM should be considered as upper bounds to the actual linewidth. Also, the noise spectrum of the *red* ECDL was measured and the integrated linewidth was 230 kHz.

Following the design presented in this thesis two additional repump lasers were built at 679 and 707 nm for the $^3P_0 \rightarrow {}^3S_1$ and $^3P_2 \rightarrow {}^3S_1$ transitions in strontium respectively as a part of another master project.

6.2 Outlook

Since the reference laser used in the beat note measurement had sidebands, it is desirable to retake the linewidth measurement when the sideband problem of the reference laser is fixed.

The ECDL housing is designed such that the external cavity length is variable. However, the influence of the cavity length on the linewidth has not been experimentally tested yet. Since the ECDL design is very robust, it could be possible that stable lasing can be achieved at larger external cavity lengths. In theory this would narrow the linewidth of the laser.

Simulations with SolidWorks show several low frequency (< 2.5 kHz) resonances of the flexure grating mount. This could be a noise source. It is worth improving the grating mount design to push the resonances to higher frequencies.

Appendix A

Circuit Diagrams

A.1 Current Controller

A.2 Temperature Controller

The temperature controller has two PID circuits. Circuit 1 is used for the cartridge heater and therefore diode (D1) is cut on the board. Circuit 2 is used for the peltier. The maximum current to both temperature control elements is set to 1 A.

A.3 PID

A.4 Connector

Appendix B

Matlab Code PSD

To obtain the power spectral density (PSD) the following Matlab code is used, which is divided into three parts. In the first part (*Read*) the data acquisition takes place. In the second part (*Process*) the data is processed. In the third part (*Scale and Plot*) the data of different datasets is scaled and plotted.

B.1 Read

```
% Data acquisition with NI datacard

% Set equal to 1 to save the obtained data
save_data = 1;

% Set sampling rate and time
Sampling_Rate = 1000000; % max 10^6
Sampling_Time = 4; % in seconds
Sample_Numbers = 20;

% Reset session and start new session
daq.reset
s = daq.createSession('ni');
s.addAnalogInputChannel('Dev2','ai0','Voltage');

% Set sampling rate and time equal to the values given above
s.Rate = Sampling_Rate;
s.DurationInSeconds = Sampling_Time * Sample_Numbers;

% Start data acquisition
[data,timestamp] = s.startForeground;
```

```
%% FFT
Fourier = abs(fft(data));
N = length(data);
freq = Sampling_Rate * (0:N/2)/N;

%% Plot Data
figure(1)
plot(timestamp,data)

figure(2)
loglog(freq, 2/N * Fourier(1:N/2+1))
xlabel('Fourier Frequency (Hz)')
ylabel('Spectral Density Noise')

%% Save Data
if save_data == 1
    Filename = strcat('NoiseSpectrum_NI_',datestr(clock,30));
    matfile = fullfile('Q:\destination', Filename);
    save(matfile,'data','timestamp','Sampling_Rate',
    'Sampling_Time','Sample_Numbers');
end
```

B.2 Process data

```
% Specify directory and name of data files
FileLocation = 'Q:\destination';
Files = ['NoiseSpectrum_NI_xx'];

% Set equal to 1 to save data
save_data = 0;

% Load data and perform FFT
for i = 1:length(Files(:,1))
    file_name = Files(i,:);
    file = fullfile(FileLocation,file_name);
    load(file)
    Data(:,i) = {data};
end

% Set number of samples
Sample_Numbers = length(data)/(Sampling_Rate*Sampling_Time);
Data_reshaped = reshape(Data{:,1},
    [Sampling_Rate*Sampling_Time,Sample_Numbers]);

% Get Autorcorrelation function
AutoCorr = autocorr(data,length(data)-1);
```

```
% Perform Welsh filter
Data_first = Data_reshaped(:,1:end-1);
Data_second = Data_reshaped(:,2:end);
Data_Welsh = [Data_first;Data_second];

% FFT with Welsh data for all samples
fft_d = fft(Data_Welsh);
N = length(Data_Welsh);
fs = Sampling_Rate;
freq = fs * (0:N/2)/N;

% Average the samples
fft_averaged = mean(abs(fft_d).^2,2);

% Plot Fourier spectrum
figure(3)
loglog(freq, 2/N * fft_averaged(1:N/2+1),'r')
xlabel('Fourier Frequency (Hz)')
ylabel('Spectral Density Noise')

% Save data
if save_data == 1
    Filename = strcat('NoiseSpectrum_Analysed_xx');
    matfile = fullfile('Q:\destination', Filename);
    save(matfile,'N','fft_averaged','freq');
end
```

B.3 Scale and Plot

```
% Specify directory and name of data files
FileLocation = 'Q:\destination';
File_1 = ['NoiseSpectrum_Analysed_24092016_Scaling_8_1'];
File_2 = ['NoiseSpectrum_Analysed_24092016_Scaling_8_2'];
File_3 = ['NoiseSpectrum_Analysed_24092016_Scaling_8_3'];
File_4 = ['NoiseSpectrum_Analysed_24092016_Scaling_8_4'];
File_5 = ['NoiseSpectrum_Analysed_24092016_Scaling_8_5'];
File_6 = ['NoiseSpectrum_Analysed_24092016_Scaling_8_6'];
File_7 = ['NoiseSpectrum_Analysed_24092016_Scaling_8_7'];
File_8 = ['NoiseSpectrum_Analysed_22092016_Scaling_6_8'];
File_9 = ['NoiseSpectrum_Analysed_22092016_Scaling_6_9'];
Files = [File_1;File_2;File_3;File_4;File_8;File_9];

LEGEND_1 = ['Locked - 10 kHz at 5 kHz'];
LEGEND_2 = ['Locked - 10 kHz at 5 kHz'];
LEGEND_3 = ['Locked - 10 kHz at 5 kHz'];
LEGEND_4 = ['Free Running - 10 kHz at 5 kHz'];
```

```
LEGEND_5 = ['Locked - 5 kHz at 41 kHz'];
LEGEND_6 = ['Locked - 10 kHz at 41 kHz'];
LEGEND_7 = ['Free Running - 10 kHz at 41 kHz'];
LEGEND_8 = ['PD Blocked'];
LEGEND_9 = ['50 Ohm'];

% Load data and perform FFT
for i = 1:length(Files(:,1))
    file_name = Files(i,:);
    file = fullfile(FileLocation,file_name);

    load(file)
    N_all(:,i) = {N};
    fft_averaged_all(:,i) = {fft_averaged};
    freq_all(:,i) = {freq};
    fft_aver_all_AC(:,i) = {fft_aver_AC};
end

% Add color map
cmap = hsv(length(Files(:,1)));

% Find scaling factors with calibration peaks
Mod = 1e3*[10, 10, 10, 10];
Pos = 1e3*[5, 5, 5, 5];
Value = [872];
Bandwidth = freq(15)/14;
Scal = 1;
Factor = Mod.^2/2;
Scaling = Factor./Scal;

for i = 1:length(Scal)
    PSD(:,i) = fft_averaged_all{i}*Scaling(i);
end

B_x = freq_all{1};
B_y = 8 * log(2)*B_x/pi^2;

f_x = linspace(110/750,1000/750,1000000);
f_1 = 1./(f_x);
f_2 = 1./(f_x).^2;

% Perform rescaling
for k = 1:length(Scal)
    PSD_linewidth = 2/N_all{k}*PSD(1:N/2+1,k);
    HS = heaviside(PSD_linewidth-B_y');
    A = HS' * PSD_linewidth/4;
    FWHM(k) = (8*log(2)*A)^0.5;
end
```

```
% Plot scaled data of multiple sets
To_plot = [1,2,3,4];
figure(2)
for j = To_plot
    loglog(freq_all{j}, 2/N_all{j} * PSD(1:N/2+1,j),'Color',cmap(j,:))
    hold on;
end
loglog(B_x,B_y,':')
hold on
loglog(f_x*630,f_1*630,':k')
hold on
loglog(f_x*430,f_2*430,':k')
xlabel('Fourier Frequency (Hz)')
ylabel('Spectral Density Noise (Hz/sqrt(Hz))')
legend(LEGEND_1,LEGEND_2,LEGEND_3,LEGEND_4,
    'B-separation line','1/f','1/f^2')
```

Appendix C

Drawings of Designs

All the dimensions are in millimeters.

C.1 ECDL Housing

C.2 Flexure Grating Mount

C.3 CMM Grating Mount

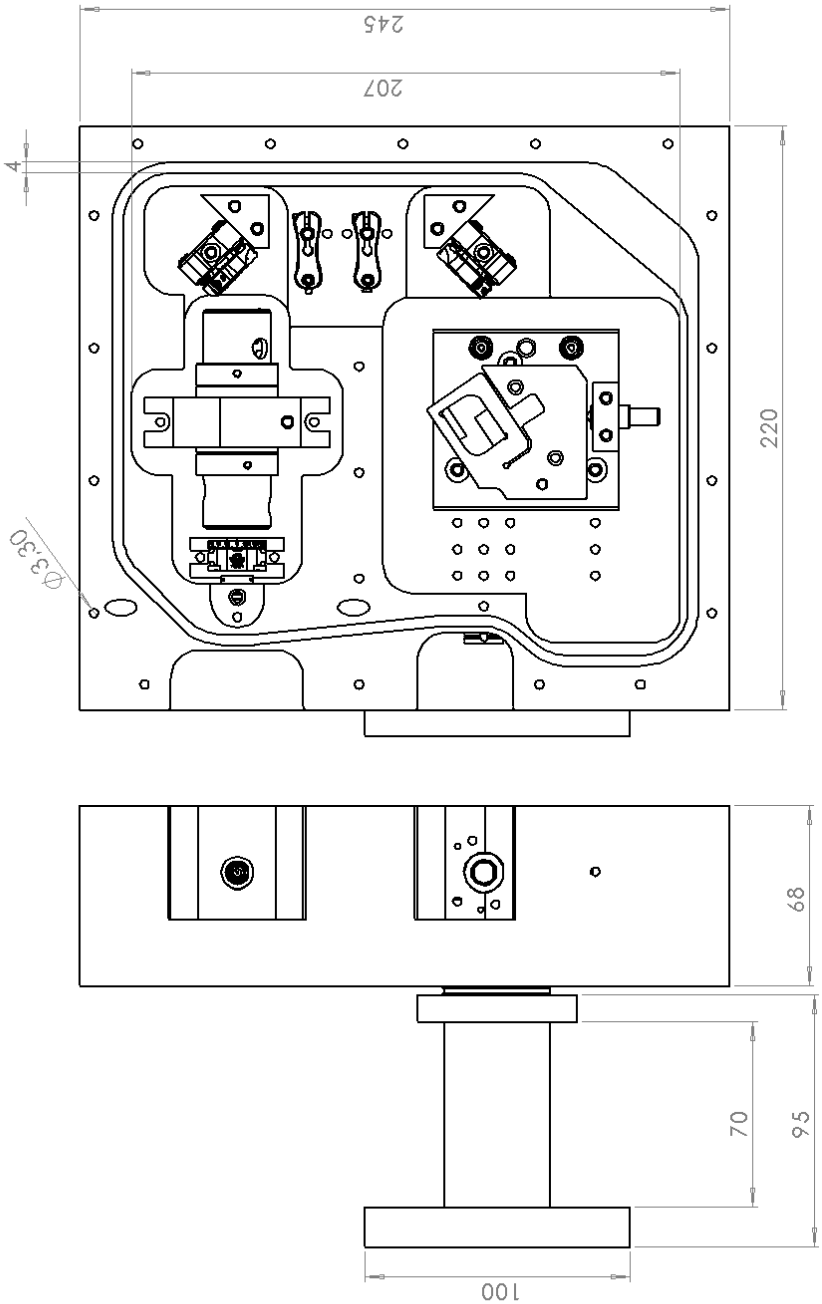

Figure C.1.1: **Drawing ECDL housing.**

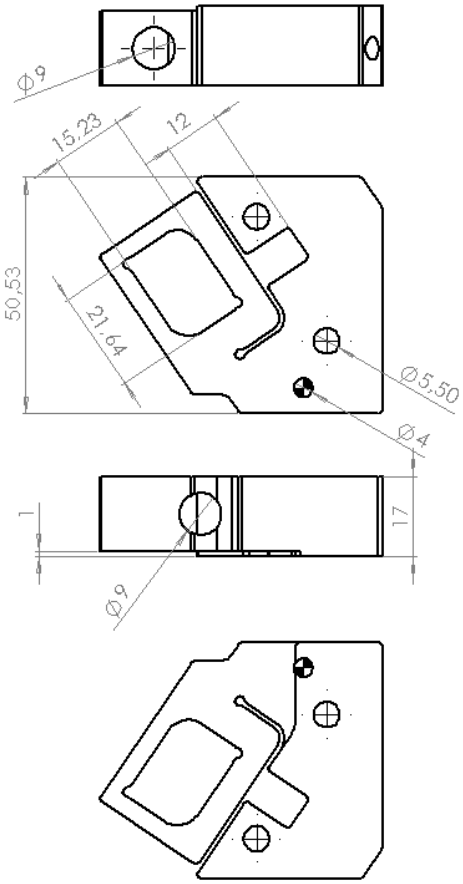

Figure C.2.1: **Drawing flexure grating mount top.**

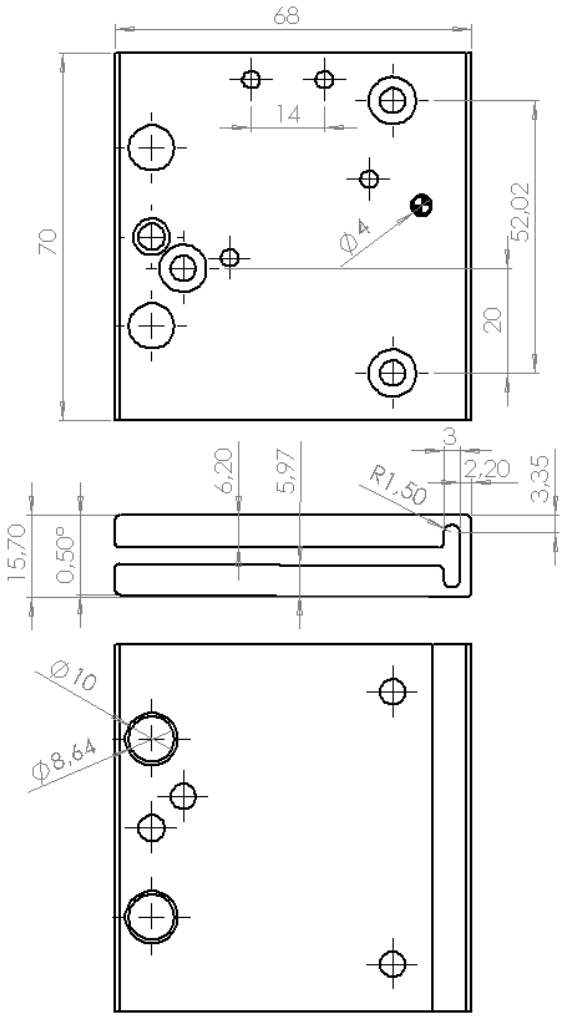

Figure C.2.2: **Drawing flexure grating mount base.**

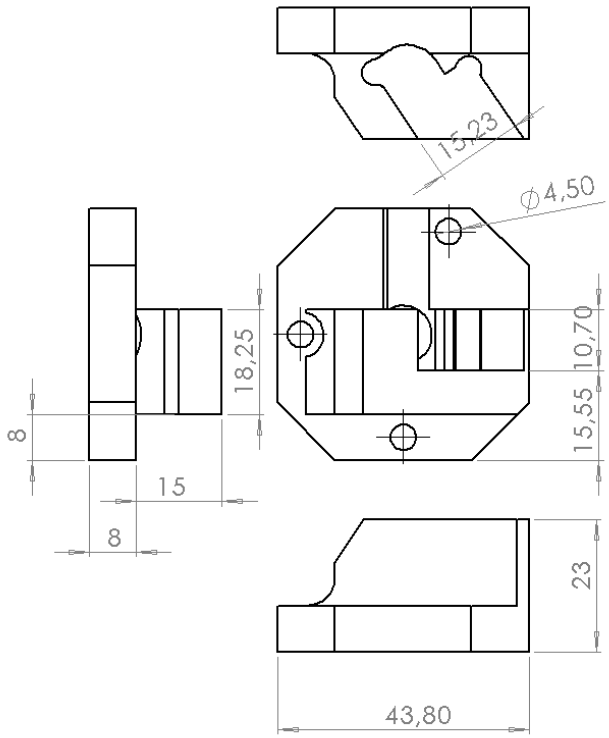

Figure C.3.1: **Drawing commercial mirror mount based grating mount.**

Bibliography

[1] T. H. Maiman, "Stimulated optical radiation in ruby," *Nature*, vol. 187, p. 493, 1960.

[2] A. Einstein, "Zur quantentheorie der strahlung," *Physik. Z.*, vol. 18, p. 121, 1917.

[3] C. J. Foot, *Atomic physics*, vol. 7. Oxford University Press, 2005.

[4] B. E. Saleh, M. C. Teich, and B. E. Saleh, *Fundamentals of photonics*, vol. 22. Wiley New York, 1991.

[5] G. van Soest and A. Lagendijk, "β factor in a random laser," *Phys. Rev. E*, vol. 65, p. 047601, 2002.

[6] A. L. Schawlow and C. H. Townes, "Infrared and optical masers," *Phys. Rev.*, vol. 112, p. 1940, 1958.

[7] T. Udem, R. Holzwarth, and T. W. Hänsch, "Optical frequency metrology," *Nature*, vol. 416, p. 233, 2002.

[8] R. M. Gagliardi and S. Karp, "Optical communications," vol. 1, p. 445, 1976.

[9] E. Ip, A. P. T. Lau, D. J. F. Barros, and J. M. Kahn, "Coherent detection in optical fiber systems," *Opt. Express*, vol. 16, p. 753, 2008.

[10] H. J. Metcalf and P. Straten, *Laser cooling and trapping of neutral atoms*. Wiley Online Library, 2007.

[11] S. Stellmer, B. Pasquiou, R. Grimm, and F. Schreck, "Laser cooling to quantum degeneracy," *Phys. Rev. Lett.*, vol. 110, p. 263003, 2013.

[12] W. Ketterle, "Nobel lecture: When atoms behave as waves: Bose-einstein condensation and the atom laser," *Rev. Mod. Phys.*, vol. 74, p. 1131, 2002.

[13] P. B. Wigley, P. J. Everitt, K. S. Hardman, M. R. Hush, C. Wei, M. A. Sooriyabandara, P. Manju, J. D. Close, N. P. Robins, and C. C. Kuhn, "Non-destructive shadowgraph imaging of ultra-cold atoms," *Opt. Lett.*, vol. 41, p. 4795, 2016.

[14] C. E. Wieman and L. Hollberg, "Using diode lasers for atomic physics," *Rev. Sci. Instrum.*, vol. 62, p. 1, 1991.

[15] J. Camparo, "The diode laser in atomic physics," *Contemp. Phys.*, vol. 26, p. 443, 1985.

[16] M. Gilowski, C. Schubert, M. Zaiser, W. Herr, T. Wübbena, T. Wendrich, T. Müller, E. Rasel, and W. Ertmer, "Narrow bandwidth interference filter-stabilized diode laser systems for the manipulation of neutral atoms," *Opt. Commun.*, vol. 280, p. 443, 2007.

[17] L. Ricci, M. Weidemüller, T. Esslinger, A. Hemmerich, C. Zimmermann, V. Vuletic, W. König, and T. W. Hänsch, "A compact grating-stabilized diode laser system for atomic physics," *Opt. Commun.*, vol. 117, p. 541, 1995.

[18] S. D. Saliba and R. E. Scholten, "Linewidths below 100 khz with external cavity diode lasers," *Appl. Opt.*, vol. 48, p. 6961, 2009.

[19] S. Bennetts, G. D. McDonald, K. S. Hardman, J. E. Debs, C. C. Kuhn, J. D. Close, and N. P. Robins, "External cavity diode lasers with 5khz linewidth and 200nm tuning range at 1.55 μm and methods for linewidth measurement," *Opt. Express*, vol. 22, p. 10642, 2014.

[20] A. I. Bawamia, G. Blume, B. Eppich, A. Ginolas, S. Spießerger, M. Thomas, B. Sumpf, and G. Erbert, "Miniaturized tunable external cavity diode laser with single-mode operation and a narrow linewidth at 633 nm," *IEEE Photonics Technol. Lett.*, vol. 23, p. 1676, Nov 2011.

[21] G. P. Agrawal and N. K. Dutt, *Semiconductor Lasers*, vol. 2nd ed., 3rd print. New York, N.Y.: Van Nostrand Reinhold, 1995.

[22] J. Ohtsubo, *Semiconductor lasers: stability, instability and chaos*, vol. 111. Springer, 2012.

[23] Y. P. Varshni, "Temperature dependence of the energy gap in semiconductors," *Physica*, vol. 34, p. 149, 1967.

[24] A. Arnold, J. Wilson, and M. Boshier, "A simple extended-cavity diode laser," *Rev. Sci. Instrum.*, vol. 69, p. 1236, 1998.

[25] C. Hawthorn, K. Weber, and R. Scholten, "Littrow configuration tunable external cavity diode laser with fixed direction output beam," *Rev. Sci. Instrum.*, vol. 72, p. 4477, 2001.

[26] H. Loh, Y.-J. Lin, I. Teper, M. Cetina, J. Simon, J. K. Thompson, and V. Vuletić, "Influence of grating parameters on the linewidths of external-cavity diode lasers," *Appl. Opt.*, vol. 45, p. 9191, 2006.

[27] A. Siegman, *Lasers.* University Science Books, 1986.

[28] S. D. Saliba, M. Junker, L. D. Turner, and R. E. Scholten, "Mode stability of external cavity diode lasers," *Appl. Opt.*, vol. 48, p. 6692, 2009.

[29] M. Born and E. Wolf, *Principles of optics: electromagnetic theory of propagation, interference and diffraction of light.* CUP Archive, 2000.

[30] L. Nilse, H. J. Davies, and C. S. Adams, "Synchronous tuning of extended cavity diode lasers: the case for an optimum pivot point," *Appl. Opt.*, vol. 38, p. 548, 1999.

[31] E. Kirilov, M. J. Mark, M. Segl, and H.-C. Nägerl, "Compact, robust, and spectrally pure diode-laser system with a filtered output and a tunable copy for absolute referencing," *Appl. phys., B Lasers Opt.*, vol. 119, p. 233, 2015.

[32] R. Raj, D. Bloch, J. Snyder, G. Camy, and M. Ducloy, "High-frequency optically heterodyned saturation spectroscopy via resonant degenerate four-wave mixing," *Phys. Rev. Lett.*, vol. 44, p. 1251, 1980.

[33] D. McCarron, S. King, and S. Cornish, "Modulation transfer spectroscopy in atomic rubidium," *Meas. Sci. Technol.*, vol. 19, p. 105601, 2008.

[34] J. H. Shirley, "Modulation transfer processes in optical heterodyne saturation spectroscopy," *Opt. Lett.*, vol. 7, p. 537, 1982.

[35] S. Stellmer, *Degenerate quantum gases of strontium.* PhD thesis, Faculty of Mathematics, Computer Science and Physics, University of Innsbruck, 2013.

[36] M. van Exter, *Noise and Signal Processing.* Lecture notes, Universiteit Leiden, 2003.

[37] C. Chatfield, *The analysis of time séries an introduction.* Chapman and hall, 1989.

[38] A. L. Lance, W. D. Seal, and F. Labaar, "Phase noise and am noise measurements in the frequency domain," *Infrared and millimeter waves.*, vol. 11, p. 239, 1984.

[39] X. Chen, *Ultra-Narrow Laser Linewidth Measurement.* PhD thesis, Faculty of the Virginia Polytechnic Institute and State University, 2006.

[40] H. Carleton and W. Maloney, "A balanced optical heterodyne detector," *Appl. Opt.*, vol. 7, p. 1241, 1968.

[41] R. Stierlin, R. Bättig, P.-D. Henchoz, and H. Weber, "Excess-noise suppression in a fibre-optic balanced heterodyne detection system," *Optical and quantum electronics*, vol. 18, p. 445, 1986.

[42] G. M. Stéphan, T. T. Tam, S. Blin, P. Besnard, and M. Têtu, "Laser line shape and spectral density of frequency noise," *Phys. Rev. A*, vol. 71, p. 043809, 2005.

[43] P. Welch, "The use of fast fourier transform for the estimation of power spectra: A method based on time averaging over short, modified periodograms," *IEEE Trans. Audio & Electroacoust.*, vol. 15, p. 70, 1967.

[44] G. D. Domenico, S. Schilt, and P. Thomann, "Simple approach to the relation between laser frequency noise and laser line shape," *Appl. Opt.*, vol. 49, p. 4801, 2010.